

Please cite as: Chen, A., Evans, B., Djordjević, and D.A. Savić (2012) A coarse-grid approach to representing building blockage effects in 2D urban flood modelling, *Journal of Hydrology*, Vol. 426-427, pp 1-16.

A coarse-grid approach to representing building blockage effects in 2D urban flood modelling

Albert S. Chen¹, Barry Evans², Slobodan Djordjević¹, Dragan A. Savić¹

¹ Centre for Water Systems, College of Engineering, Mathematics and Physical Sciences, University of Exeter, UK

² Department of Geography, College of Life and Environmental Sciences, University of Exeter, UK

Abstract

The latest information and communications technology has enabled flood modelling in urban areas using high quality terrain data to simulate the detailed flow dynamics in local areas. However, the computational cost rises exponentially as the resolution goes finer. The advance of computing hardware is still a limiting factor for large-scale area or risk/uncertainty analysis modelling with fine resolution that describes the details of building features. Grid coarsening is the straightforward way to reduce the computing efforts for 2D flood modelling. The traditional approach to grid coarsening usually takes the average elevation of a fine grid as the new terrain model for the coarse grid. This approach often results in loss of information that introduces errors to modelling. In this study, the building features in coarse grids were abstracted using the building coverage ratio (BCR) and the conveyance reduction factor (CRF) parameters in a 2D model to simulate flooding in urban areas. The outcome of 2D case studies showed the proposed model can minimise the errors due to terrain averaging and provide a much better accuracy of modelling results at a marginally increased computing cost.

Keywords: Urban Inundation Model (UIM), building blockage effect, building coverage ratio (BCR), conveyance reduction factors (CRFs)

Introduction

Accuracy and efficiency are two major indicators in evaluating the performance of flood numerical models. Higher accuracy can be obtained by: (1) considering more terms in the governing equations to explain the detailed behaviour of hydraulic phenomena; (2) adopting numerical methods with higher order precision and calculations that introduce less machine error to restrict discretization inaccuracy; and/or (3) using finer spatial and temporal resolutions to present local attributes. On the other hand, the efficiency can be enhanced by: (1) neglecting less significant equation terms to reduce the complexity; (2) improving numerical schemes to speed

up the solving procedures; (3) reducing problem size or dimensionality of modelling to decrease the computation efforts; and/or (4) using faster hardware to save the computing time. These two aims (accuracy and efficiency) are often in conflict with each other and a compromise is commonly sought after in practical applications.

The recent development of remote sensing technology has widened the availability of digital terrain models (DTMs) and digital elevation models (DEMs). In the last decade, Light Detection and Ranging (LiDAR) has been adopted to obtain high quality terrain information – for example at present the UK Environment Agency LiDAR data cover 62% of England and Wales with horizontal spatial resolution ranging from 0.25m to 2m and a vertical accuracy between 5cm and 15cm. The use of these detailed DTMs from the LiDAR data enables flood models to better describe the flow behaviour around buildings. Therefore, data availability no longer represents a significant limit to improvements in accuracy of numerical modelling. The increase of model resolution, however, results in the growth of grid cell numbers (to the square of the resolution ratio). As a consequence, the number of steps for temporal progress increases because the time computational step decreases with grid size to ensure model stability. For example, a case study using a 0.4 km x 0.96 km area with 2m grid resolution requires 4 – 308 minutes of computing time for a 5 hour event simulation using existing 2D inundation models (Néelz and Pender, 2010). The wide range of computing times was due to the choice of time steps and the number of iterations within each time step, the efficiency of numerical algorithms, the use of multi-processing, the hardware specification and other computational overhead costs for modelling.

Many parallel computing techniques, including Message Passing Interface (MPI), Open Multi Processing (Open-MP) and Graphical Processing Unit (GPU), have been applied to speed up 2D inundation modelling (Hankin et al., 2008; Neal et al., 2010). Lamb et al. (2009) demonstrated that the GPU application can speed up the inundation modelling more than 100 times compared to the traditional CPU-based model on a standard desktop PC with a little additional hardware investment. Bates et al. (2010) recently found that adding the inertia term to the diffusive inundation model LISFLOOD-FP can improve the model stability to allow greater time steps in modelling. Together with the implementation of MPI and Open-MP, the latest version

of LISFLOOD-FP performed much faster than its previous versions. Nevertheless, the growth of high resolution terrain data is much quicker than the increase of computing capacity for real time or large scale modelling. The limitations of available computing resources, therefore, still restrict the applications when very detailed information or risk-based analysis is required over large areas.

Increasing the cell size can effectively improve efficiency, but also can cause reduction in details i.e. loss of information about surface features. For instance, elevations of 'macro objects' (e.g., building, bridges, etc.) represented in fine grid models would be smeared or completely removed when the grid is coarsened. Hence, the local flow phenomena could not be reflected properly in coarse grid applications (McMillan and Brasington, 2007). Methods to keep the required detailed information within coarse grid calculations are therefore important to retain the accuracy.

The IMPACT project (Alcrudo, 2004) has presented several techniques to simulate the blockage effect of buildings in urban areas by using: (1) local friction based representation of buildings; (2) the bottom elevation technique; and (3) vertical walls. The three approaches were compared with laboratory experiments and the applicability of these methods was validated. Néelz and Pender (2007) modified the roughness values of coarse grids to account for the obstructions and found that the sub-grid treatment (McMillan and Brasington, 2007; Yu and Lane, 2006b) is needed for the parameterisation of coarse grids in certain cases. Guinot and Soares-Fraza (2006) accounted for the building blockage effect using porosity in a 2D overland flow model with unstructured grids to avoid grid refinement around buildings in order to capture the local flow dynamics.

How to make the most of the available high quality information in urban flood modelling in order to provide accurate and timely information for risk management has become an important issue to be explored. In this paper, a new approach to coarse grid modelling in urban areas is proposed to represent the blockage effect on surface flow caused by buildings. The information from fine grid cells is extracted and simplified by using three parameters for a coarse-grid resolution cell to reflect the cell's porosity. The area occupied by buildings is expressed as the building coverage ratio (BCR) and the cross sections blocked by buildings on the cell interfaces are

described by the two conveyance reduction factors (CRFs). The next section explains the details of the methodology, followed by the applications of the proposed model to a real case study. Further model comparisons and discussions are given in the subsequent section. Finally, the key findings are summarised and conclusions drawn.

Methodology

Urban inundation model (UIM)

UIM, a 2-D non-inertia model based on the Saint Venant equations, was developed for simulating the overland flow propagation on alluvial plains with mild natural topography (Chen et al., 2005). The acceleration and inertial terms are neglected because they are often relatively small compared to gravity and friction terms. The original governing equations are written as

$$\frac{\partial d}{\partial t} + \frac{\partial ud}{\partial x} + \frac{\partial vd}{\partial y} = q \quad (1)$$

$$\frac{\partial (d + z)}{\partial x} + \frac{n^2 u \sqrt{u^2 + v^2}}{d^{4/3}} = 0 \quad (2)$$

$$\frac{\partial (d + z)}{\partial y} + \frac{n^2 v \sqrt{u^2 + v^2}}{d^{4/3}} = 0 \quad (3)$$

where, Eq. (1) is the continuity equation and Eqs. (2) and (3) are the momentum equations in the horizontal Cartesian directions x and y ; d is the water depth [m]; u and v are the velocity components in the x and y directions, respectively [m/s]; z is the water surface elevation [m]; n is Manning's roughness coefficient; q is the rate of water entering or leaving ground surface per unit area, including the excess rainfall, the upstream catchment inflows, the inflow and outflow of sewer networks, and the overland flow drained by hydraulic facilities [m/s].

UIM adopts an explicit scheme to solve equations (1)-(3). Adaptive time stepping is implemented to speed up the calculation (Chen et al., 2007). The optimum time step is determined according to the Courant-Friedrichs-Lewy condition to prevent the water travelling more than one cell distance in a single step, and the transferrable volume of a cell to avoid the 'chequer board' oscillations. A similar methodology was used in the 2D cell storage models (Hunter et al., 2005; Yu and Lane, 2006a) to limit

the flow exchanged between cells within a time step, or adjusting the time steps to capture the detailed flow dynamics.

Buildings occupy considerable parts in urban areas, and their walls usually exclude deluges from the interior spaces during flooding. Water thus flows around buildings rather than into or through them, unless their entrances are left open or the water level exceeds the crest heights of entrances. Fine grid modelling is commonly combined with using the roof elevations or with raising the ground elevations where buildings are located to characterise the physical situation in overland flow modelling (Fewtrell et al., 2008; Wang et al., 2010). The grid resolution is often lower than the scale of buildings such that the positions and elevations of buildings are properly represented by fine cells, however, the solution is computationally expensive. When the grid size is much greater than the building scale, the ground elevation is normally used along with increased local roughness in numerical simulation; yet the results are often too coarse to describe local phenomena, which are required for practical applications.

Building coverage ratio (BCR)

A building might occupy a significant, but not the total area within a computational cell, which could have a similar or slightly larger size than the building scale. Neither the ground elevation nor the roof elevation is appropriate to interpret that condition. Figure 1 shows examples of building representation on computational cells. The building edges may be perfectly aligned with the fine cell boundaries (Figure 1-a) such that the roof elevations can describe the locations of buildings properly. When the coarse grid is adopted, the average of roof and ground elevations will smear the space between buildings (Figure 1-b) and consequently change the hydraulic behaviour. In that situation, neither the use of roof elevations (Figure 1-c), which reduces the conveyance section of flow, nor the use of ground elevations (Figure 1-d), which allows extra cross section area, can provide accurate description of the terrain feature.

Hsu et al. (2000) introduced the BCR, $\alpha = A_b / A$ [-], to account for the reduced cell area for modelling, where A_b is the building area [m²] and A is the cell area [m²],

as shown in Figure 2. The building is regarded as a rectangle with closed walls parallel to the boundaries of the containing grid cell and the flux cannot move across or enter the building. The effective area within a cell, which allows for flow storage and movement, is calculated as $(1 - \alpha)A$ and the conveyance widths, in both x and y directions, are reduced by the ratio $(1 - \sqrt{\alpha})$. The continuity equation is then rewritten as

$$(1 - \alpha) \frac{\partial d}{\partial t} + \frac{\partial \left[(1 - \sqrt{\alpha})ud \right]}{\partial x} + \frac{\partial \left[(1 - \sqrt{\alpha})vd \right]}{\partial y} = q \quad (4)$$

Although Liggett (1975) concluded that the variation of channel width does not alter the momentum equation, the solution of water depth in the modified continuity equation changes the pressure and the friction terms such that BCR has implicit influence on the momentum equations.

The parameter BCR accurately estimates the effective area of a computational cell, which is close to the reality; nevertheless, in many cases the sole use of BCR cannot describe the flow regimes properly. The problem is due to the fact that various alignments of buildings inside a grid may produce diverse flow possibilities at the same BCR values. Figure 3 illustrates several examples of the grids that all have the identical BCR = 0.25, but different building placements or shapes, hence should result in different flows across them. The building location inside a cell obviously affects the flow condition. For instance, in Figure 3 the building in cell b fully blocks the flux across the upper boundary and partially obstructs the flux in the x direction. On the other hand, the flow over cell c, which has the same building dimensions but a different placement, has no chance of passing through the left cell boundary and is partially obstructed in the y direction because of the building.

Conveyance reduction factors (CRFs)

Since BCR does not clarify the building alignments within cells, the numerical model gives equivalent flow behaviour for same BCR, which results in inadequate predictions. To distinguish different situations, the dimensionless CRFs, β_x and β_y , were adopted to represent the maximum occupancy ratios of buildings on the computational grid boundaries in x and y directions, respectively (Figure 4). If the

possible flow out of each coarse grid cell is considered, the *CRF* values are given in Table 1 obtained at each boundary. The BCR value α is independent from CRFs except for some rectangular building cases with walls parallel to the grid boundaries, where $\alpha = \beta_x \beta_y$. Accordingly, the conveyance widths for flux in the x and y directions are reduced by the ratios $(1 - \beta_x)$ and $(1 - \beta_y)$, respectively. The continuity equation now becomes:

$$(1 - \alpha) \frac{\partial d}{\partial t} + \frac{\partial [(1 - \beta_x) u d]}{\partial x} + \frac{\partial [(1 - \beta_y) v d]}{\partial y} = q \quad (5)$$

The combination of BCR and CRFs describes more details about the building situations such that the model is capable of predicting the flow more realistically.

Applications

Both 1D and 2D hypothetical case studies were adopted to test model application. The 1D case studies were aimed at validating the UIM model against the HEC-RAS model. The latter solves the 1D steady flow using the standard step method with much finer resolution. Furthermore, the case studies were used to test the coarse grid treatments when accounting for building blockage effects. The 2D case studies investigated different coarse grid resolutions and compared different grid coarsening approaches to examine the model performance. 2D flows in real urban area were also simulated to test the model's ability to represent buildings.

1D case studies

Two case studies were selected for 1D model applications. Both studies simulated 1D steady flow such that the results obtained by using HEC-RAS were taken as benchmark solution. Two grid resolutions, 5m and 10m, were adopted in UIM simulations, which were referenced as UIM 5M and UIM 10M cases, respectively. Two indicators, the root mean square error (RMSE) of maximum flood depths and the flood volume (FV), were chosen to assess the model performance. The RMSE illustrates the absolute errors of water depths between UIM and HEC-RAS results, along the street's central longitudinal profile. The FV is the total flood volume stored in the domain.

Case study 1-1 (model validation)

The first study case was a straight street, 30 m wide and 300 m long, as shown in Figure 5, with horizontal bed. The constant upstream inflow was $1 \text{ m}^3/\text{s}$ and the downstream boundary water depth was fixed at 0.2 m; the Manning roughness was 0.06, which was widely used for 2D modelling (Hunter et al., 2008; Tayefi et al., 2007; Yu and Lane, 2006b). The longitudinal profile of water depths, obtained by HEC-RAS, UIM 5M, and UIM 10M simulations, along street centres are displayed in Figure 6.

Table 2 shows that UIM 5M gave better agreement with HEC-RAS, however, the performance of UIM 10M was also close to the HEC-RAS results. UIM tended to underestimate the water depths slightly, and the differences were larger at upstream reach. Besides the simplified governing equations, which omit inertial terms, another factor contributing to the errors was the hydraulic radius calculation in UIM. As a shallow-water equation model, UIM uses the flow depth to represent the hydraulic radius for determining the discharge, whereas HEC-RAS considers the total wet perimeter in discharge calculation (Brunner, 2002). The assumption in UIM implied the absence of walls roughness, and resulted in smaller water depths in UIM simulations. The HEC-RAS simulation with negligible walls roughness ($n=0.0001$), as shown in **Error! Reference source not found.**, demonstrated a closer agreement with the UIM result.

Case study 1-2 (model comparison)

The difference between this case study and the previous one was the addition of buildings in the middle section of the street, as shown in Figure 7. The building section was simulated as a channel with sudden contraction and a sudden expansion in HEC-RAS. As the previous case study has revealed that the absence of walls roughness in UIM might introduce errors, the wall roughness was set as negligible in HEC-RAS to minimise this source of error in the following discussions.

The buildings are located on both sides at the middle section of the street, each block 5m wide, 120m long and 3m high. The building alignment is easily set by rising the ground elevation which is occupied by buildings in the UIM 5M case. For the UIM 10M cases, however, the same technique was inappropriate because the buildings

occupy a part of the grid area. If the grid cells were completely elevated, the building area would be over-estimated and the conveyance width of the street reduced by 50%. Using the average elevation would result in the same effect. Various approaches were tested to account for the building blockage effect, which are reported in the following sections. **Error! Reference source not found.** shows the longitudinal profile of water depths, obtained by HEC-RAS, UIM 5M, and four UIM 10M simulations, along street centres.

Case 1-2 (a) UIM 5M

The grid with 5m resolution was used in UIM simulation. The building scale is equal to the grid size such that the replacement of ground elevation by the roof elevation properly reflects the reality. The performance indicators listed in Table 4 show that the UIM 5M was in very good agreement with the benchmark.

Case 1-2 (b) UIM 10M (partially increased roughness)

The grid with 10m resolution was used in UIM simulation. The roughness of cells with buildings was doubled to 0.12, which is significantly larger than the normal value range. The resulting RMSE was slightly higher than the UIM 5M, however, the FV was 15% higher than that of the benchmark because the technique assumes that the full grid area remains available for water storage.

Case 1-2 (c) UIM 10M ($\alpha = 0.50$)

The grid with 10m resolution was used in UIM simulation. The BCR of cells partially occupied by building was set to $\alpha = 0.5$ for simulation. The CRFs were then calculated as $\sqrt{\alpha} = 0.71$, which decreased the conveyance width by 42% in the longitudinal direction. The result shows that FV values were closer to the benchmark than in the *UIM 10M (partially increased roughness)* case since the building areas were deducted from the cells. However, the results exhibit a greater RMSE because of the overestimated CRF along the longitudinal direction.

Case 1-2 (d) UIM 10M ($\alpha = 0.25$)

The result of *UIM 10M ($\alpha = 0.50$)* case shows that the CRF was overestimated along the longitudinal direction. To calculate the CRF along the longitudinal direction properly, the BCR for cells that contain buildings was set to $\alpha = 0.25$. Therefore, the reduction of conveyance width in the longitudinal direction was accurately

represented using $\sqrt{\alpha} = 0.50$. The treatment provided results close to the benchmark in term of the RMSE. Nevertheless, the extra storage volume available due to the underestimated BCR resulted in a significantly higher FV error.

Case 1-2 (e) UIM 10M ($\alpha = 0.50, \beta_x = 0.5, \beta_y = 0.0$)

The use of BCR only (without CRF) is limited in describing correctly the influence of building alignments within cells. Estimating of neither the conveyance width nor the storage volume is sufficiently accurate, such that the independent CRF parameters are required. In the case study, β_x of cell boundaries that are occupied by buildings was set to 0.5, whereas the β_y was set to 0.0 because the buildings are not situated on the boundaries of the central cells. The BCR α of 0.5 was used in order to reflect the actual area covered by buildings. Both RMSE and FV for the 10m grid show closer performance to the ones of the UIM 5M case than UIM 10m approaches.

2D case studies

The coarse grid modelling was investigated with different grid coarsening approaches using a 2D hypothetical terrain model. The 400m x 100m 'ski run' DEM surface, shown in Figure 9, consists of three sections. The first and the last 100m long sections have a slope of 0.005 and the middle 200m section has a milder slope of 0.002. The northern and southern boundaries are closed and the eastern (outflow) boundary is open. A lateral discharge, shown in Figure 10, was introduced at the western boundary and was distributed uniformly over a sixty meter swath (thirty meters either side of the centre line bisecting the y-axis where $x = 0$). The normal flow was set as the downstream condition at the eastern boundary. These boundary conditions were applied to ensure the propagation of flow along the surface from west to east. An "E" shaped wall with 4m height is located in the middle section of the domain and the building's orientation is such that it had a closed face to the incoming surface flow.

The effects of grid coarsening via the bare DEM without the wall were investigated first, then the cases with the walls included were simulated using: (1) the DEM averaged with the building roof elevation (averaged DEM), and (2) the averaged bare DEM with the BCR and CRFs (BCR & CRFs), to analyse the flows around a building

feature. The original DEM with 1m resolution was applied to provide the benchmark solution. The bare DEM was averaged and re-sampled into 4m, 5m, 10m, and 20m grids. The choice of the resolutions ensured that all grids had exactly the same modelling domain, however, the alignment of the building feature with the cell boundaries differed from grid to grid. Figure 11 shows the alignment of the cell boundaries in the region near the wall. The west edge of the wall fits with the cell boundary in 5m and 10m resolutions, but is aligned in the middle of the cells in 4m and 20m resolutions. Similar conditions were kept on the north and the south edges.

The model performance was evaluated based on the RMSE of the maximum flood depths of coarse grids against the 1m benchmark solution, for the overall domain and the middle section. The error distribution maps and the flood depth profiles along the central line ($y=50$) in the x direction were compared to assess the overall accuracy.

Case Study 2-1 (bare DEM)

The bare DEM without the E wall was tested first to investigate the influence of grid coarsening. Figure 12 shows the maximum flood depths during the simulation for

each grid cell in a raster map format.

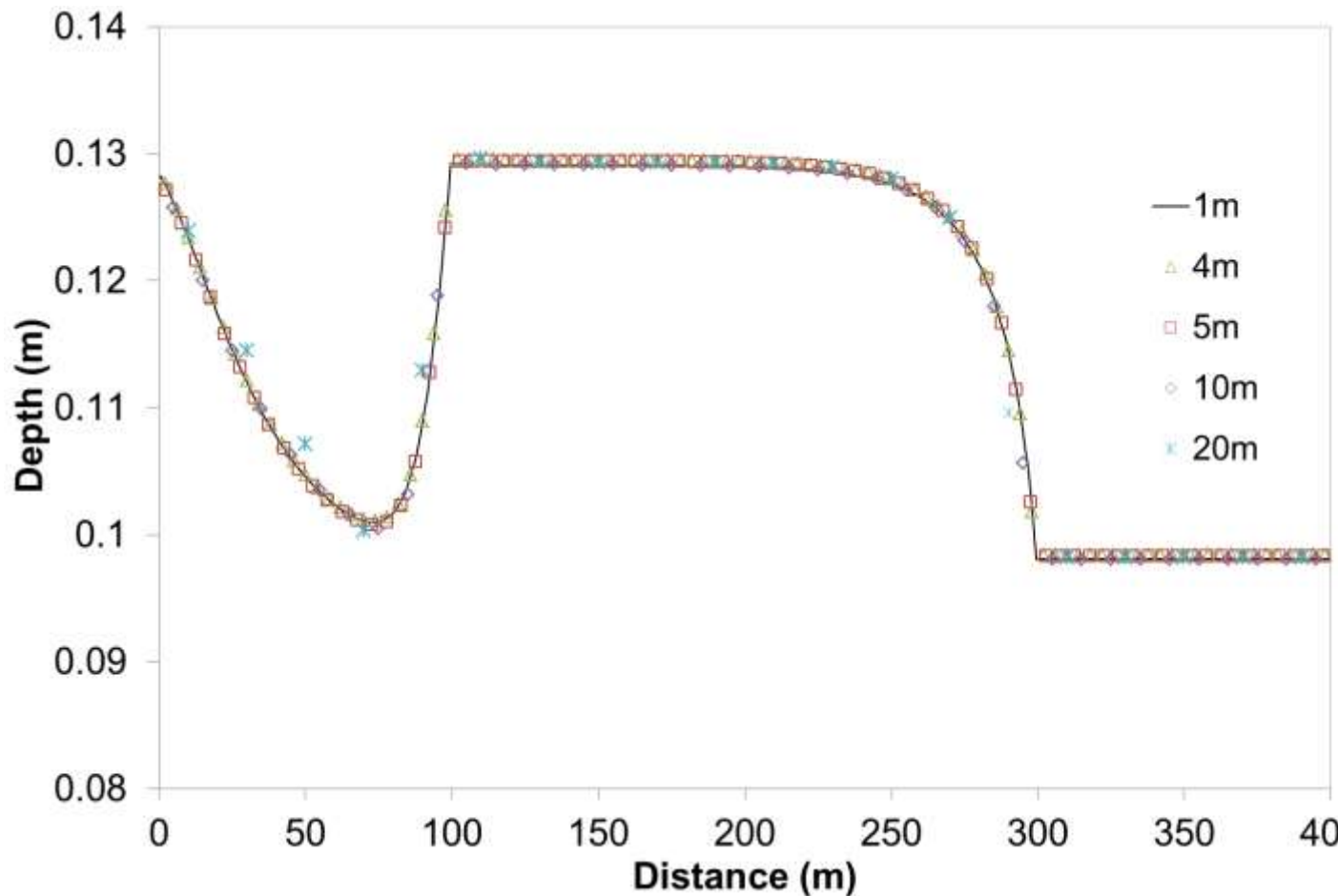


Figure 13 shows the maximum flood depth profiles along the central line of the domain in the x direction. The lateral flow input from the western boundary initially spreads across the surface in the first section ($0m < x < 100m$). The depth drops from 0.128m to 0.101m ($x=75m$) and then increases due to the backwater effect of the flow in the middle section ($100m < x < 300m$). The flood depth stays at 0.128m until $x=250m$ where rapid decrease appears because of the change of bed slope at $x=300m$. The depth remains at 0.098m in the final section ($300m < x < 400m$).

All the coarse grids generated results are similar to the 1m benchmark. The modelling results of coarse grids were remapped back to 1m resolution and flood depths were compared against the benchmark. The error distribution map, shown in Figure 14, indicates that greater errors occurred in the first section where the lateral inflow was introduced, and in the two regions near the location where the bed slope changed. The results obtained by coarse grid gave the same average flood depth over the area of a coarse cell, whereas the 1m benchmark produced spatially varied

depths for the fine-grid cells in the same area. Therefore, the banding effect could be observed on the error distribution maps. The flood depths in the downstream part of a coarse cell tend to be overestimated in coarse grid modelling, while the upstream part was underestimated (

Table 5). The table lists the RMSE of coarse grid modelling results for the overall domain and for the region of the middle section against the 1m benchmark solution. The RMSE for the middle section are less than 2.5 mm for all coarse grids, which shows that the grid resolution has limited influence on modelling results.

Case Study 2-2 (averaged DEM)

The cases where the E-shape wall existed were further examined to compare the different grid coarsening approaches in reflecting the blockage effects. The traditional approach that adopted the average elevation of terrain and buildings was tested first. The effect of averaging DEM solely was investigated using the different sizes of group coarsening windows. The roof elevation was averaged with the ground elevation to reflect the existence of buildings. Figure 15 shows the maximum flood depth profile along the central line in the x direction and Figure 16 shows the error distribution maps. The flood depths increase rapidly in the region $100\text{m} < x < 150\text{m}$ due to the blockage effect of the building. The depths drop to 0m in the region $150\text{m} < x < 176\text{m}$ occupied by the building, and raise again in the region $176\text{m} < x < 250\text{m}$, where the water flow propagates back behind the building. The same flow behaviour as the bare DEM case was observed in the region $x > 250\text{m}$.

Case Study 2-3 (BCR & CRFs)

BCR and CRFs were adopted to describe the building features within a coarse cell. The *BCR* value for each coarse cell was calculated based on the area ratio occupied by a building. The *CRF* values were determined based on the ratio between the building width (on the interface between two cells) and the width of the cell interface. The elevation of a coarse cell was calculated as the average elevation of the fine cell elevations, which were not occupied by buildings in the coarse cell area. By representing buildings separately and by coarsening the bare DEM dataset, the

spreading effects of buildings due to averaging with the roof elevation were completely removed.

Figure 17 shows the maximum flood depth profile along the central line in the x direction and Figure 18 shows the error distribution maps. The errors of flood depths in 4m, 5m and 10m grids were smaller than those obtained using coarse grid DEM, and the error bands surrounding the building were also removed. However, the 20m grid underestimated the flood depths in front of the building and overestimated in the region behind the building. The representation of the blockage effect appears not to be captured correctly at the 20m resolution.

2D real case model

The previous analyses show that the BCR & CRFs approach enables a more accurate representation of flood depths within a terrain and the localised representation of surface flow paths. The averaged DEM and the BCR&CRFs approaches were further compared using a real case terrain model to see if the new methodology can perform better than the traditional approach.

A 300m x 300m LiDAR tile at 1m resolution with terrain and building roof elevations, which is shown in Figure 19, was adopted for the benchmark modelling. 3m, 6m, and 12m grids were used to produce the averaged DEM for coarse grid modelling. For the BCR & CRFs approach, the difference between DTM and DEM was analysed to generate the building raster grid for determining the BCR and CRFs. Another approach to generating the building raster grid and calculating those parameters would be to overlap the DTM with the building layer from the Ordinary Survey Mastermap, when the data is available. A 1-hour extreme rainfall event with constant intensity of 60mm/hr was applied directly to the surface as the input and the simulation time was kept at ninety minutes. This allowed a thirty-minute period for water movement across the surface after the rainfall stopped.

Figure 20 shows the distribution of the maximum flood depth on the 1m resolution benchmark model. The pattern of water distribution reveals two areas where there was significant ponding of surface water. These regions are highlighted as regions A and B. The flood depths in region A and B were approximately 40cm and 90cm, respectively. The figure shows that water accumulated in region A and then flowed

through a narrow alleyway in the direction of the location of region B, and accumulated within that region. Some of the surface water partially trapped in this region travelled again in a north-westerly direction through an alleyway or eventually around the building in a north-easterly to north direction when the surface depths were large enough.

Case Study 3-1 (averaged DEM)

In the 3m grid modelling with averaged DEM, the fine scale alleyways between buildings were immediately lost resulting in excessive accumulation of water in regions A and B (Fig. 21-a). The overestimation in region A was directly a result of the loss of the key transmissible alleyway that conveyed water across to region B. Although region B was no longer receiving inflow from region A, the loss of this region's alleyways meant that the only exit routes were around the building features. This coupled with the spread of the buildings results in a greater area for trapping water and leads to an increase in water depths within this region.

Generalising further to 6m resolution not only led to the loss of alleyways between buildings, but also caused the narrowing of street channels that convey surface water (Fig. 21-c). Therefore, the water depths within these street networks were overestimated. For the alleyways between building and the areas that the buildings were spread to, the water can no longer access these regions and the flood depths were thus underestimated.

The modelling result of the 12m grid, as expected, was the least accurate (Fig. 21-e). The error distribution pattern reveals that most of the surface flow was prevented or severely limited due to the large degree of building spread. Thus, large areas of depth underestimations and sporadic regions of accumulated depth overestimations can be seen in the result.

Case Study 3-2 (BCR & CRFs)

The 3m grid modelling with BCR & CRFs, as shown in Figure 21-b, preserved the alleyways between buildings and ensured more accurate results than the averaged DEM approach. This improvement was reflected in the inspection of regions A and B where the errors fluctuated around the zero within these regions.

The modelling result of 6m grid with BCR & CRFs, shown in Figure 21–d, revealed that the flood depths within region A were underestimated. This underestimation was a result of small holes within previously blocked alleyways (pathways 1 and 4 in **Error! Reference source not found.**) being created due to the positioning of the coarsening window and the subsequently calculated CRFs. **Error! Reference source not found.** shows a partial section of region A and the direction of flow between cells where no flow was possible before in the benchmark model. The CRFs were smaller than one on the cell boundaries, together with the BCR that was less than one, which allowed the water to enter the cell from one side and leave at the others, although the internal fine cells did not permit the transfer. This led to an increase of water moving towards region B reflected by the overestimation of maximum flood depths in the error analysis map.

The 12m grid with BCR & CRFs approach led to a significant underestimation of water depths within regions A and B. The loss of water within these regions was a direct consequence of the coarsening window's size and position. This enabled water to fully encompass buildings in one of the buildings' dimensions leading to bisections of the coarse grids. This bisection was supposed to stop the water movement, but the flow paths, the arrows shown in Figure 23, were created in the BCR & CRFs approach. The CRFs were smaller than 1.0 on those cell boundaries that allowed the flow routing through building features.

Discussion

1D case studies

Case study 1-1 shows that wall roughness needs to be accounted for in high-resolution studies, especially when the flow depth is large enough that the shallow-water equations assumptions do not hold. When using the water depth in the rough calculation of hydraulic radius for fine grid applications, the approximated hydraulic radius is greater than the one that considers the full wetted perimeter. The discharge derived by the momentum equation, for a single grid with both sides parallel to flow direction and attached to building walls, is amplified by the ratio:

$$r_q = \left(\frac{\Delta x + 2d}{\Delta x} \right)^{\frac{5}{3}}$$

where, r_q is the amplified discharge ratio [-]; d is the water depth [m]; Δx is the grid size [m].

Figure 24 shows the relationships between the amplified discharge ratio and the water depth for different grid sizes. The calculated discharge is doubled when water depth reaches 0.26 m for grid size $\Delta x = 1$ m. Even for the coarser grids with $\Delta x = 5$ m and 10m, the simplified hydraulic radius calculation for a flow depth of 0.3m caused 21% and 11% of discharge over-estimations, respectively. For the steady flow cases, the simplification resulted in 12% and 6% of under-estimation of flow depth. Although a fine grid has its both sides attached to building walls only when encountering a narrow street, the wall roughness on single grid side still needs careful consideration. The water depth errors between the UIM 5M results and HEC-RAS benchmark of the case study 1-1 were smaller than the above-mentioned value, which was up to 12%, because of just two of the six grids in a single cross section were next to the walls. The two grids had only one boundary that was attached to the walls such that the under-estimation of flow depth was smaller than in the case where a grid had both sides attached to buildings. The cross-sectional averaging also reduced the error.

In case study 1-2, the roughness of grids containing buildings in the *UIM 10M (partially increased roughness)* case did not show any general trend, thus providing no objective criteria for its adjusting. The tuning of the roughness value to achieve the minimum discrepancy in model results needed several runs and the optimum values differed from case to case. Although a proper setting produced good performance in the RMSE, the huge disagreement in the FV existed as a consequence of not considering the area occupied by buildings, which was the major disadvantage of the approach.

2D case studies

The bare DEM case demonstrated that the grid resolution had little effect on the flow in the middle section when the E-shape building did not exist. The errors in the middle section in the averaged DEM and the BCR & CRFs cases were obviously greater than those in the bare DEM case. The existence of the building caused the

blockage effect and the grid coarsening methods introduced errors, depending on the details of the building features described.

The averaged DEM approach

The terrain elevations of cells in the averaged DEM cases were raised as the consequence of averaging with the building height. The height of the building was set high so that the averaged elevations of the coarse cells blocked the flow. Hence, the building area spread out and increased in coarse grids. Although the approach reflected the blockage effect in coarse grid simulations, the results between different grid resolutions varied significantly.

For the 4m grid, the elevated terrain led to approximately 80% increase in the building area (the sum of black and shaded areas in Figure 11). This in turn reduced the conveyance width on both north and south sides of the building, decreasing each from 30m to 28m. In contrast, the increase of building area in 5m grid occurred only inside the building and the conveyance width was not reduced on either side of the building. Therefore, the blockage effect was more significant in the 4m resolution than in 5m resolution, which led to overestimated flood depths in the upstream area of the building. Greater underestimation occurred in the bands next to the buildings because those coarse cells had higher elevation such that the resulting flood depths were zero.

For the 10m grid, the E wall became 3x4 cells with higher elevation such that the backwater could not enter inside the building. Therefore, substantial errors occurred in the area. Like with the 5m grid, the building edges for modelling on the west, north and south sides remained the same as for the 1m benchmark, hence, smaller errors were introduced in the upstream area. For the 20m grid, the averaged DEM extended the building area by 10m toward west, north and south sides. The elevations of the six cells occupied by the wall were too high to allow the flow to pass through. This caused more blockage effect in the area in front of the building, and larger underestimation of depth for the area occupied by the building.

The overall analysis of generalisation effects reveals that the spreading of features will result in either the loss of information around the building or proportionally large

Please cite as: Chen, A., Evans, B., Djordjević, and D.A. Savić (2012) A coarse-grid approach to representing building blockage effects in 2D urban flood modelling, *Journal of Hydrology*, Vol. 426-427, pp 1-16.

errors within its vicinity. The averaged DEM results in an overall increase in surface depths as available space for surface flow is reduced. As the spreading of buildings is dependent on the coarsening window position, coarser resolutions may *by chance* give more accurate results than fine scales.

Table 6 lists the RMSE of the averaged DEM modelling results compared to the benchmark solution. The results showed that the 5m and 10m grids provided a more accurate representation of flood depths than the finer 4m grid. The RMSE values in the middle section were greater than the overall RMSE. The DEM averaging with building roof elevation expanded the building area and, therefore, overestimated the blockage effect and resulted in large error in the middle section.

The BCR & CRFs approach

The alignment of buildings within a coarse cell obviously affected the modelling results. The selections of the reference point and the cell size to construct a coarse grid are critical for describing correctly the flow movement. In practice, the orientation and location of buildings are often irregular such that the optimum setting of a coarse grid for modelling would be very difficult to reach. To improve the accuracy of modelling, the BCR and CRFs were introduced to describe the features of buildings within a coarse cell. In the BCR & CRFs grids, some coarse cells were only partially occupied by buildings. This partial occupancy in a standard coarse-grid approach would cause spreading of the building features into the terrain, which the BCR and CRF methodology avoided, as shown by previous examples.

Comparing the error distribution maps of the averaged DEM and the BCR & CRFs cases, the large underestimation errors in the bands next to the building, which were caused by the building spread such as in the 4m and 20m coarse grid cases, were completely removed. The errors in the upstream area next to the building were also reduced (except the 20m grid case), because the conveyance widths were properly reflected in coarse grids.

The 5m grids in the averaged DEM and the BCR & CRFs cases had identical results in the upstream area of the building. The same condition was found in the results of the 10m grids due to the specific positioning of the coarse grid. Figure 25 displays the CRF values of the cell interfaces on the edge of building in the 10m grid. The coarsening window for 5m and 10m grids encompassed the building in such a way that the outer boundary of each coarse cell facing the incoming surface flow fit cell boundaries. This resulted in a CRF value of one on the cell interface meaning that from this direction the adjacent cell was inaccessible.

The reason that the 20m grid failed to improve the accuracy was due to the assumption that the approach did not take into account the situation when a building bisects a coarse cell. In the benchmark, the water from the west was redirected to the channel on either north or south side because the building blocked the flow path. The water can only enter the building via the opening on the east side. In the coarse grid modelling, except for the 20m grid, the CRF values for the cell interfaces on building edges were set to 1.0. This prevented the flow entering the building from west, north and south sides. The water can flow back via the east side where the CRF values were smaller than one.

Figure 26 shows the CRF_x values of the cell interfaces in the neighbourhood of the building in the 20m grid. None of the values was set to 1.0, according to the definition that only takes the occupancy of buildings on the cell interfaces into account without considering the bisectioning inside a cell. Hence, the water can directly travel from west to east regardless of the existence of the wall, which divided the cell into two separated parts. The blockage effect disappeared in the modelling, therefore, the flood depths were underestimated in the upstream area in front of the building. For the area inside the building, the flood depths were overestimated because the water can flow through the building without any obstacle.

The RMSE in Table 7 clearly show that the BCR & CRFs approach provided better accuracy than the averaged DEM approach (

Table 6). The 4m grid outperformed the rest coarse grids because the building features were precisely described. The RMSE in the middle section of the whole domain were similar to the overall RMSE, which means the BCR & CRFs approach can maintain the accuracy of modelling without introducing additional errors. Unlike the averaged DEM case, the 4m grid provided a more accurate representation of flood depths than the coarse grids in the BCR & CRFs approach. The results, except for the 20m grid, were independent from the locations of buildings in a cell. The reference point and the grid resolution had much less influence on the modelling accuracy.

2D real case model

Although 1m resolution LiDAR was applied to the case study, the alleyways between buildings were not appropriately described in the benchmark model. The narrow alleyways were blocked in modelling because of the orientations and the locations of building edges. The alleyways that were not parallel to the cell boundaries were represented as zigzag pixels among high buildings, as shown in **Error! Reference source not found.**, such that the water cannot travel through them because the model can only compute the flow perpendicular to cell boundaries.

The non-orthogonal arrangement of buildings in real world made the grid coarsening more difficult to fit building edges with coarse cell boundaries. The averaged DEM approach further smeared away those alleyways that flow could access and narrowed down the street channels because of the spreading of building. Consequently, more errors occurred in the modelling results.

The BCR & CRFs approach preserved those accessible alleyways in the benchmark model such that better agreement was achieved in the modelling results. However, it also opened some of those blocked alleyways (pathways 1 and 4 in **Error! Reference source not found.**) due to the CRFs on the cell interfaces that were smaller than one. The pathway was created in a coarse cell regardless of the flow path was, i.e., blocked because of the zigzag representation of fine cells. Some pathways remained blocked in the model because the union of the building wall projections on both sides of the cell interfaces resulted in CRF values equal to one. Though the inconsistent setting, which created pathways between buildings,

comparing to the benchmark model that blocked the pathways, the BCR & CRFs modelling cleared the narrow pathways between buildings which may lead to better representation of the real physical situation.

Computational efficiency

The 2D E wall case studies were used herein for comparison of the computing efficiency. The models were executed on the high performance cluster Zen of the University of Exeter. We adopted a dual quad-core 2.83GHz Intel Xeon E5440 Harpertown node and 16GB RAM for simulations. For the 1m resolution benchmark the computational time required was more than 7.5 hours for a simulation, as shown in Table 8, while the 4m grids took just above 2 minutes for computing. The 1m benchmark simulation took an extraordinary time because the optimum time steps reduced quadratically (Bates et al., 2010) to less than 0.001s to maintain a stable solution without the 'chequer board' oscillations.

In general, the BCR & CRFs approach required a marginally longer computing time for 4m and 5m grids than the averaged DEM approach, nevertheless, the gain was the significantly improved accuracy of modelling results. For the 10m grid, the blockage effect was less significant in the BCR & CRFs approach because the inner areas of the building were available for storage. This resulted in smaller gradient of water surface behind building and speeded up the simulation. For the 20m grid in the BCR & CRFs approach, the blockage effect of building was not simulated such that the gradient of flow surface became milder than the averaged DEM approach. The smoother surface allowed the UIM to solve the equations using greater time step such that the simulation was quicker.

Conclusions

The approach presented in this paper demonstrated the possibility of increasing accuracy of flood modelling results within a coarse grid model. Using BCR alone will allow for the interpretation of available storage space for water; however, the use of BCR only (without CRFs) does not guarantee a good prediction, due to the building alignments within grids typically not being represented well. The over-reduction of the conveyance width and/or over-estimation of the storage volume are the main factors

that cause simulation errors. The BCR & CRFs approach simplifies the key features of building within a coarse grid into three additional parameters for modelling, which enhance the description of the available storage space within a coarse grid cell and the effective conveyance width between neighbouring cells. The extensive computing efforts in fine grid modelling and the loss of information in coarse grid modelling are avoided. Although marginally less computationally efficient than the BCR only approach, the new method improves significantly the coarse grid modelling accuracy. Unlike the tuning of roughness, the settings of BCR and CRFs can be done based on DEM and land uses data, which is straightforward, objective and with practical physical meaning.

The traditional averaged DEM approach is highly sensitive to the reference point and the cell size in establishing the coarse grid. The optimal selections of these parameters are difficult to reach in practical applications. In contrast, the BCR & CRFs approach is independent from the building orientation and location within a coarse cell. The case study demonstrated the approach is even capable of improving the terrain description of narrow alleyways between buildings. However, the current methodology is limited to the scenario where a building bisects a coarse cell, which blocks the internal flow movement. Failure to consider this scenario in the case studies showed significant errors in modelling results. We believe that further work on a multilayer approach, which could describe the features of the separate regions *within* a coarse cell, is required to improve the model accuracy.

Acknowledgements

The work is supported by the EPSRC funded project “Flood Risk Management Research Consortium (FRMRC) Phase 2 (Grant EP/F020511/1)”. The authors are also grateful to the Environment Agency for providing the LiDAR data.

References

- Alcrudo, F., 2004. Mathematical modelling techniques for flood propagation in urban areas. IMPACT Project technical report (http://www.samui.co.uk/impact-project/AnnexII_DetailedTechnicalReports/AnnexII_PartB_WP3/Modelling_techniques_for_urban_flooding.pdf).
- Bates, P.D., Horritt, M.S., Fewtrell, T.J., 2010. A simple inertial formulation of the shallow water equations for efficient two-dimensional flood inundation modelling. *Journal of Hydrology*, 387(1-2): 33-45.

- Brunner, G.W., 2002. HEC-RAS River Analysis System Hydraulic Reference Manual. CPD-69, Hydrologic Engineering Center, US Army Corps of Engineers Davis, CA.
- Chen, A.S., Djordjević, S., Leandro, J., Savić, D., 2007. The urban inundation model with bidirectional flow interaction between 2D overland surface and 1D sewer networks, NOVATECH 2007, Lyon, France, pp. 465-472.
- Chen, A.S., Hsu, M.H., Chen, T.S., Chang, T.J., 2005. An integrated inundation model for highly developed urban areas. *Water Sci Technol*, 51(2): 221-229.
- Fewtrell, T.J., Bates, P.D., Horritt, M., Hunter, N.M., 2008. Evaluating the effect of scale in flood inundation modelling in urban environments. *Hydrological Processes*, 22(26): 5107-5118.
- Guinot, V., Soares-Frazao, S., 2006. Flux and source term discretization in two-dimensional shallow water models with porosity on unstructured grids. *Int J Numer Meth Fl*, 50(3): 309-345.
- Hankin, B., Waller, S., Astle, G., Kellagher, R., 2008. Mapping space for water: screening for urban flash flooding. *Journal of Flood Risk Management*, 1(1): 13-22.
- Hsu, M.H., Chen, S.H., Chang, T.J., 2000. Inundation simulation for urban drainage basin with storm sewer system. *Journal of Hydrology*, 234(1-2): 21-37.
- Hunter, N.M. et al., 2008. Benchmarking 2D hydraulic models for urban flooding. *Proceedings of the Institution of Civil Engineers-Water Management*, 161(1): 13-30.
- Hunter, N.M., Horritt, M.S., Bates, P.D., Wilson, M.D., Werner, M.G.F., 2005. An adaptive time step solution for raster-based storage cell modelling of floodplain inundation. *Adv Water Resour*, 28(9): 975-991.
- Lamb, R., Crossley, M., Waller, S., 2009. A fast two-dimensional floodplain inundation model. *Proceedings of the Institution of Civil Engineers-Water Management*, 162(6): 363-370.
- Liggett, J.A., 1975. Basic Equations of Unsteady Flow. In: Mahmood, K., Yevjevich, V. (Eds.), *Unsteady Flow in Open Channels*. Water Resources Publications, P.O. Box 303, Fort Collins, Co. USA, Fort Collins, pp. 29-62.
- McMillan, H.K., Brasington, J., 2007. Reduced complexity strategies for modelling urban floodplain inundation. *Geomorphology*, 90(3-4): 226-243.
- Neal, J.C., Fewtrell, T.J., Bates, P.D., Wright, N.G., 2010. A comparison of three parallelisation methods for 2D flood inundation models. *Environmental Modelling & Software*, 25(4): 398-411.
- Néelz, S., Pender, G., 2007. Sub-grid scale parameterisation of 2D hydrodynamic models of inundation in the urban area. *Acta Geophysica*, 55(1): 65-72.
- Néelz, S., Pender, G., 2010. Benchmarking of 2D Hydraulic Modelling Packages Heriot Watt University, Edinburgh.
- Tayefi, V., Lane, S.N., Hardy, R.J., Yu, D., 2007. A comparison of one- and two-dimensional approaches to modelling flood inundation over complex upland floodplains. *Hydrological Processes*, 21(23): 3190-3202.
- Wang, X., Cao, Z., Pender, G., Neelz, S., 2010. Numerical modelling of flood flows over irregular topography. *Proceedings of the Institution of Civil Engineers-Water Management*, 163(5): 255-265.
- Yu, D., Lane, S.N., 2006a. Urban fluvial flood modelling using a two-dimensional diffusion-wave treatment, part 1: mesh resolution effects. *Hydrological Processes*, 20(7): 1541-1565.
- Yu, D., Lane, S.N., 2006b. Urban fluvial flood modelling using a two-dimensional diffusion-wave treatment, part 2: development of a sub-grid-scale treatment. *Hydrological Processes*, 20(7): 1567-1583.

Table 1. CRF values for example building layouts (where BCR = 0.25) in Figure 3

Case	CRFx (East)	CRFx (West)	CRFy (North)	CRFy (South)
A	0.00	0.00	0.00	0.00
B	0.25	0.25	1.00	0.00
C	0.00	1.00	0.25	0.25
D	0.25	0.25	0.00	0.00
E	0.50	0.50	0.50	0.50
F	0.00	0.50	0.50	0.00

Table 2. Performance of the UIM simulations, compared to the HEC-RAS benchmark, for case study 1-1.

	HEC-RAS	UIM 5M	UIM 10M
RMSE (mm)	-	1.54	2.38
FV (m ³)	2,411	2,398	2,390

Table 3. Performance of the UIM simulations, compared to the HEC-RAS with negligible walls roughness benchmark, for case study 1-1.

	HEC-RAS with negligible walls roughness	UIM 5M	UIM 10M
RMSE (mm)	-	1.06	1.95
FV (m ³)	2,407	2,398	2,390

Table 4. Performance of the UIM simulations, compared to the HEC-RAS with negligible walls roughness benchmark, for case study 1-2.

	HEC-RAS with negligible walls roughness	UIM 10M				
	(a) UIM 5M	(b) n=0.12	(c) $\alpha = 0.50$	(d) $\alpha = 0.25$	(e) $\alpha = 0.50$ $\beta_x = 0.5$ $\beta_y = 0.0$	
RMSE (mm)	-	1.26	2.83	17.1	1.74	1.74
FV (m ³)	2,206	2,175	2,537	2,309	2,374	2,199

Table 5. RMSE of the coarse grid modelling results against the benchmark for the bare DEM case

	4m	5m	10m	20m
Overall domain RMSE (mm)	0.93	1.12	2.35	4.45
Middle section RMSE (mm)	0.56	0.70	1.30	2.44

Table 6. RMSE of the coarse grid modelling results against the benchmark for the averaged DEM case

	4m	5m	10m	20m
Overall domain RMSE (mm)	13.2	4.70	10.1	37.9
Middle section RMSE (mm)	19.2	6.76	14.2	53.1

Table 7. RMSE of the coarse grid modelling results against the benchmark for the BCR & CRFs case

	4m	5m	10m	20m
Overall domain RMSE (mm)	1.16	1.45	3.10	15.0
Middle section RMSE (mm)	1.16	1.43	3.05	20.6

Table 8. Model properties and simulation time for the 2D averaged DEM and BCR & CRFs approaches

Cell size (m)	General (No. Cells)	CPU time (s)	
		Averaged DEM	BCR & CRFs
1	40,000	27,004	-
4	2,500	125.5	199.3
5	1,600	67.5	68.7
10	400	5.59	4.82
20	100	2.42	1.15

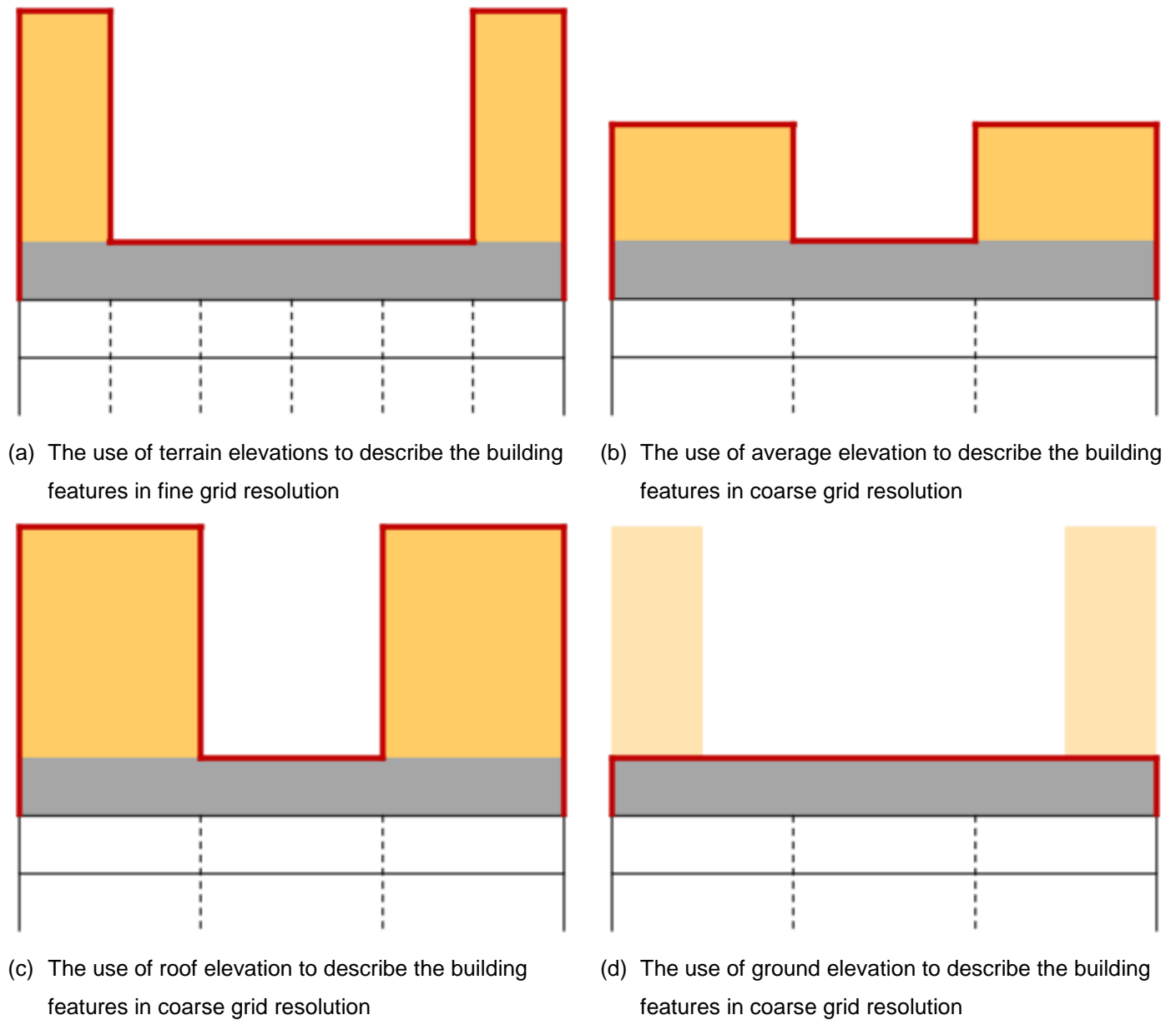


Figure 1. Schematic for a computational grid which contains buildings

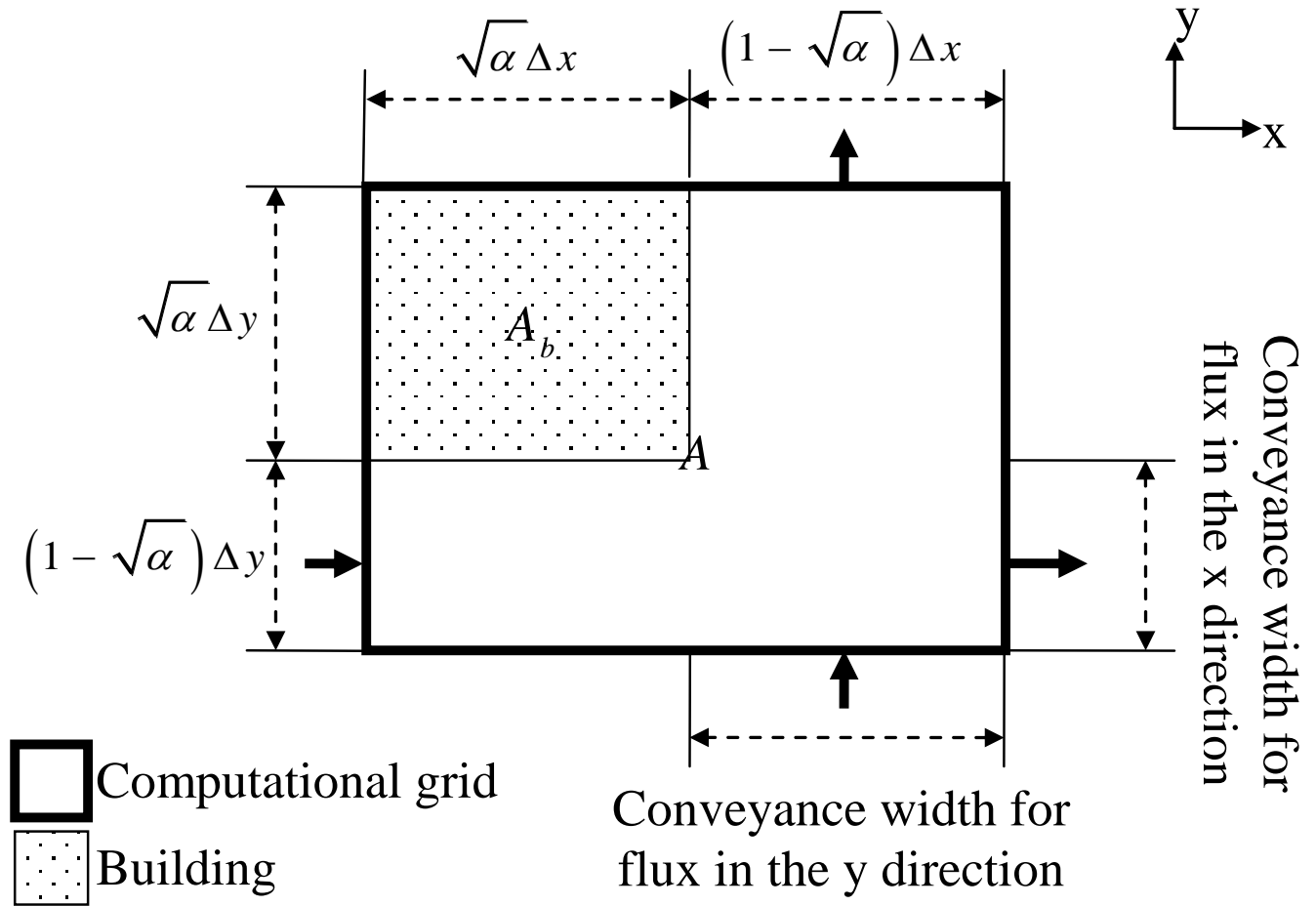


Figure 2. Schematic for a computational grid which contains buildings

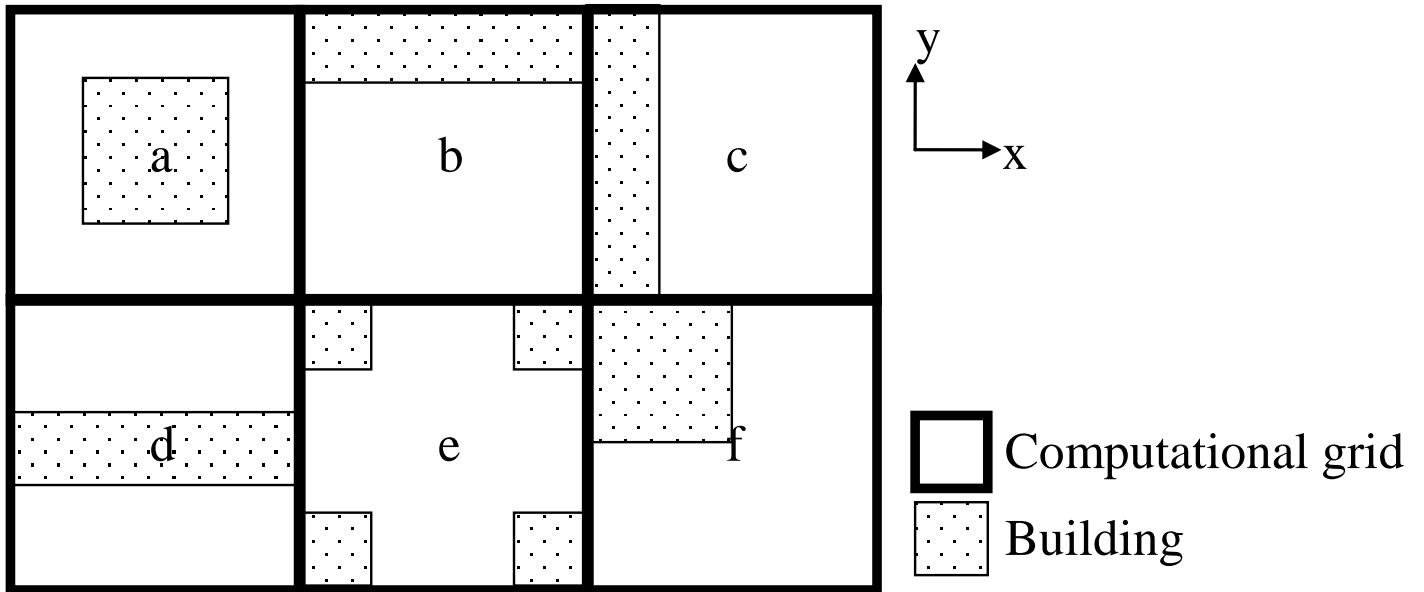


Figure 3. The computational grids with various building alignments

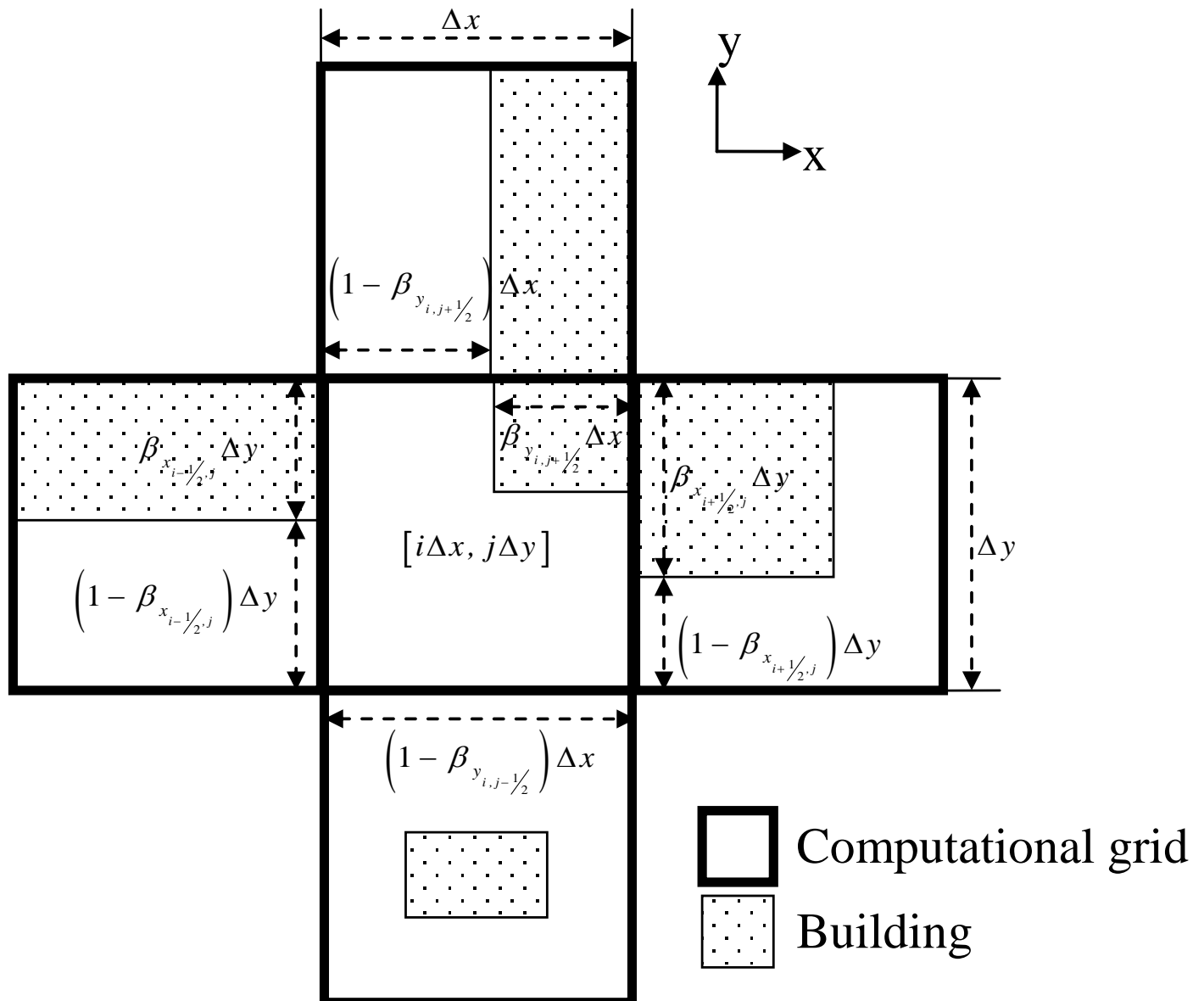


Figure 4. The determinations of the CRFs for a computational grid are based on the building alignments within itself and its neighbourhood grids

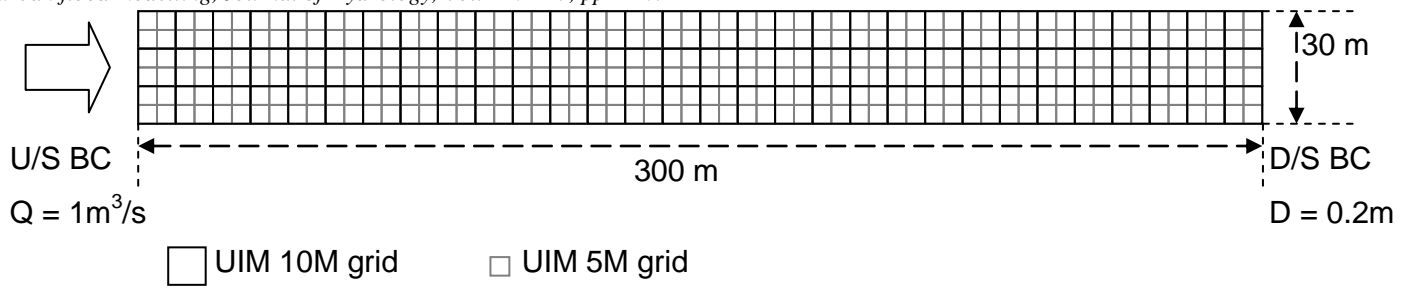


Figure 5. The plan view, grids and U/S and D/S boundary conditions of study case 1

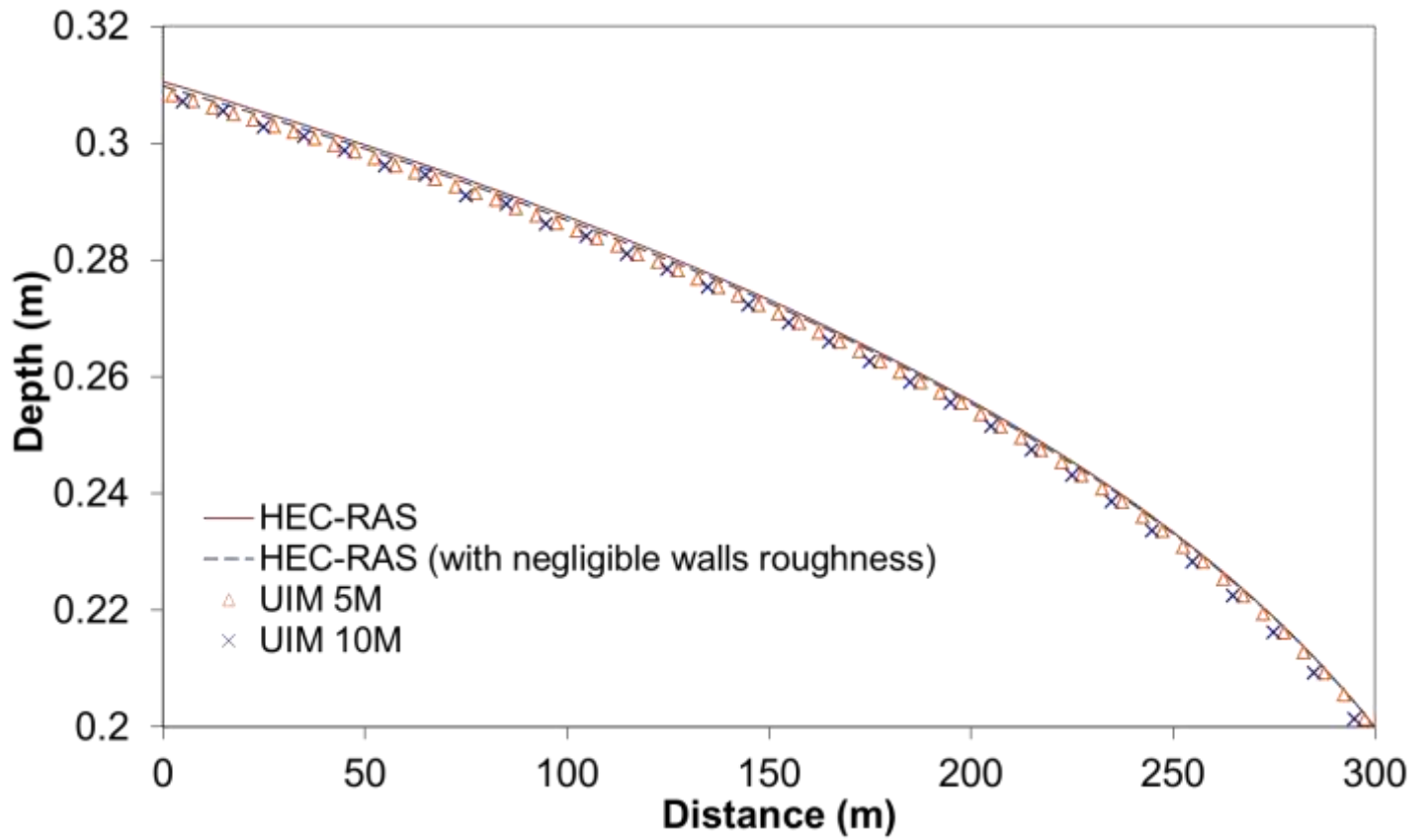


Figure 6. The longitudinal profiles along the street centres obtained by HEC-RAS, HEC-RAS with negligible walls roughness, UIM 5M and UIM 10M simulations

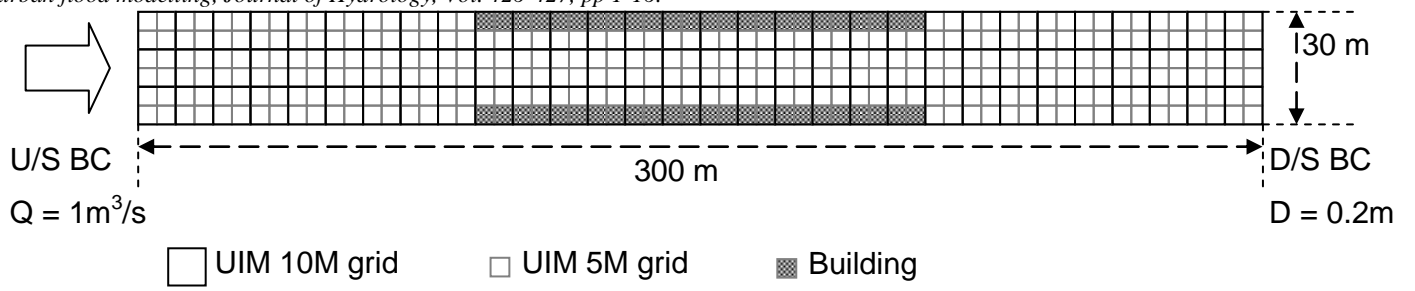


Figure 7. The plan view, grids and U/S and D/S boundary conditions of study case 2

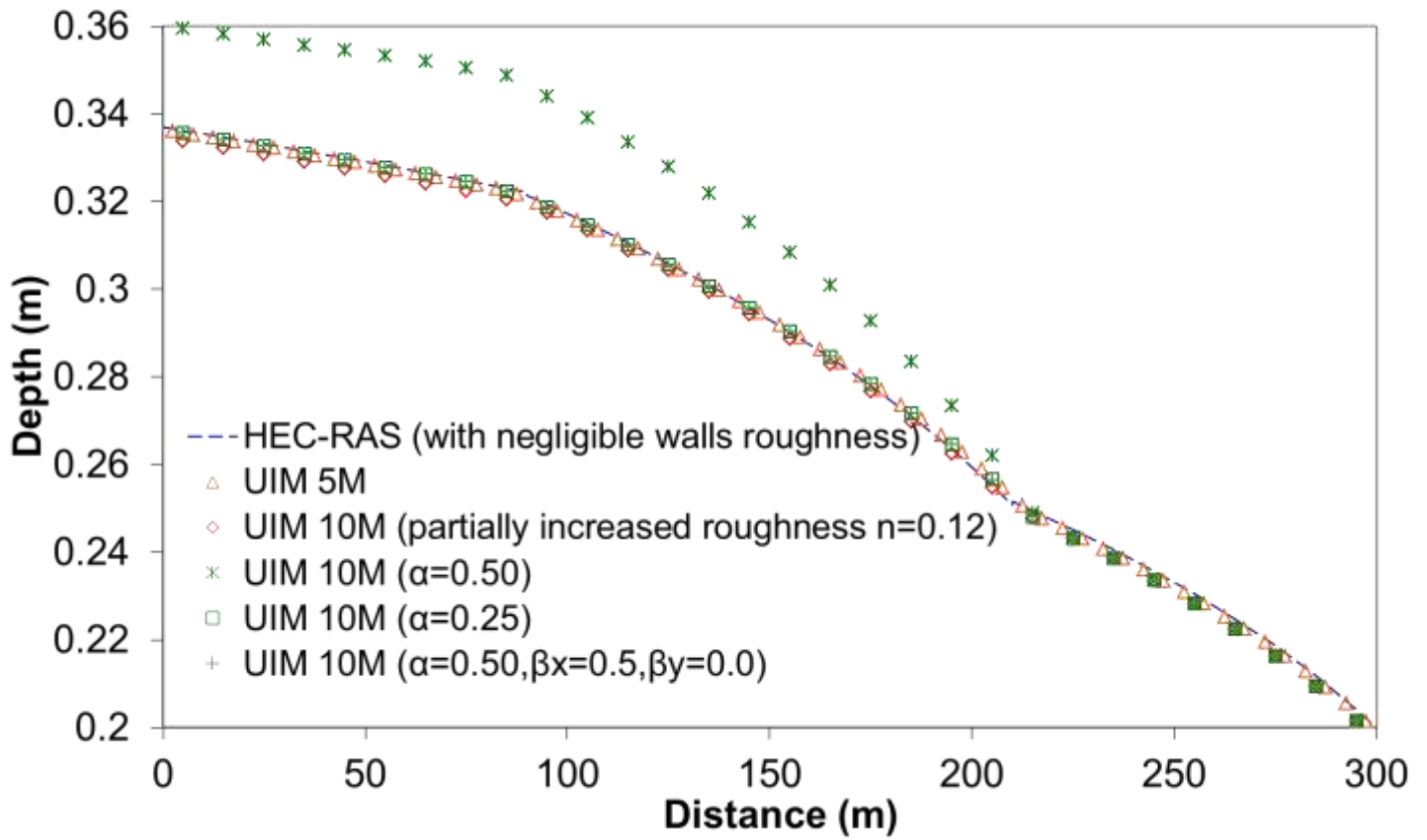


Figure 8. The longitudinal profiles along the street centres obtained by HEC-RAS, UIM 5M and four UIM 10M simulations

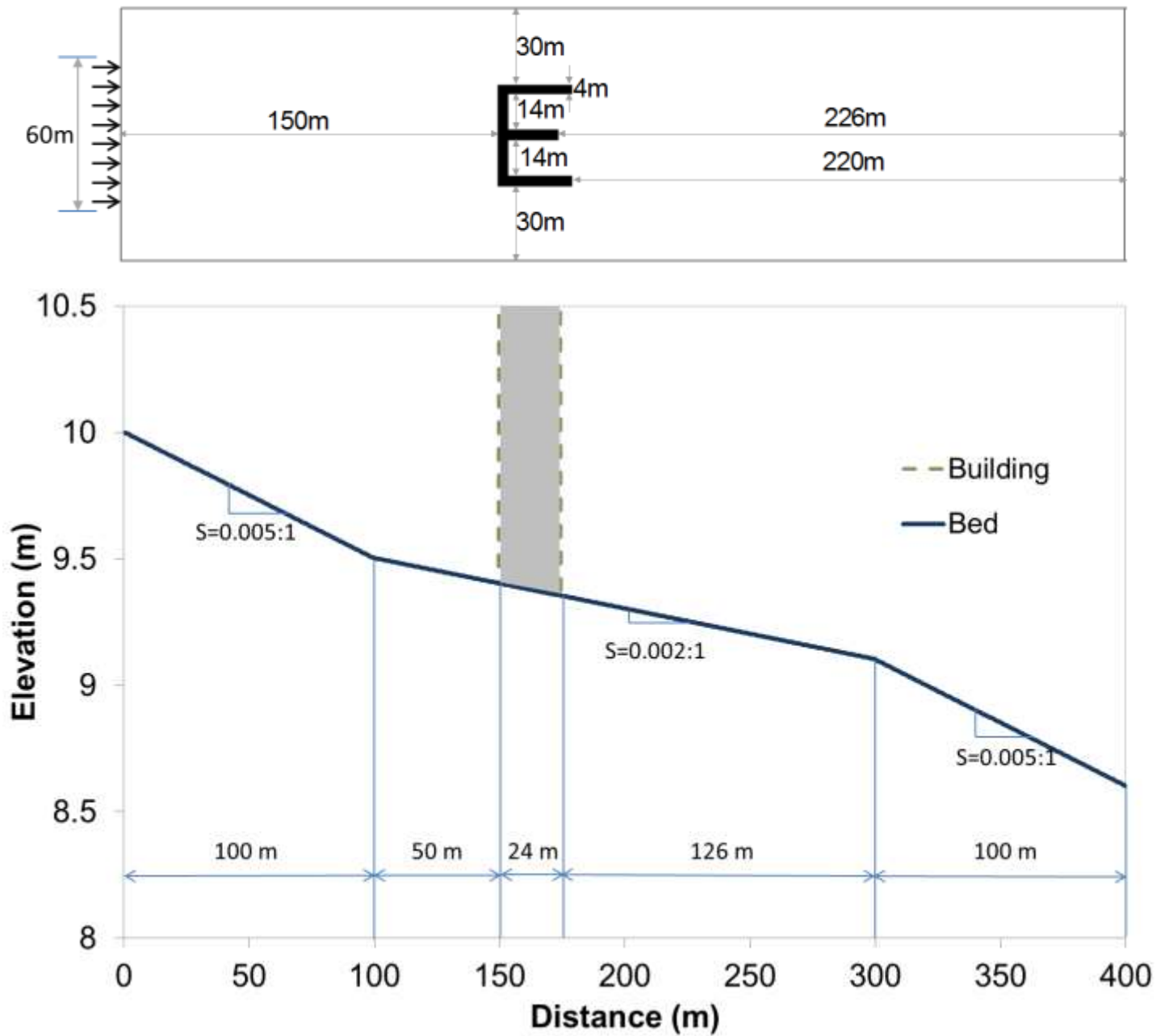


Figure 9. The plain view (up) and the longitudinal elevation profile (down) along the central line of the 2D case study

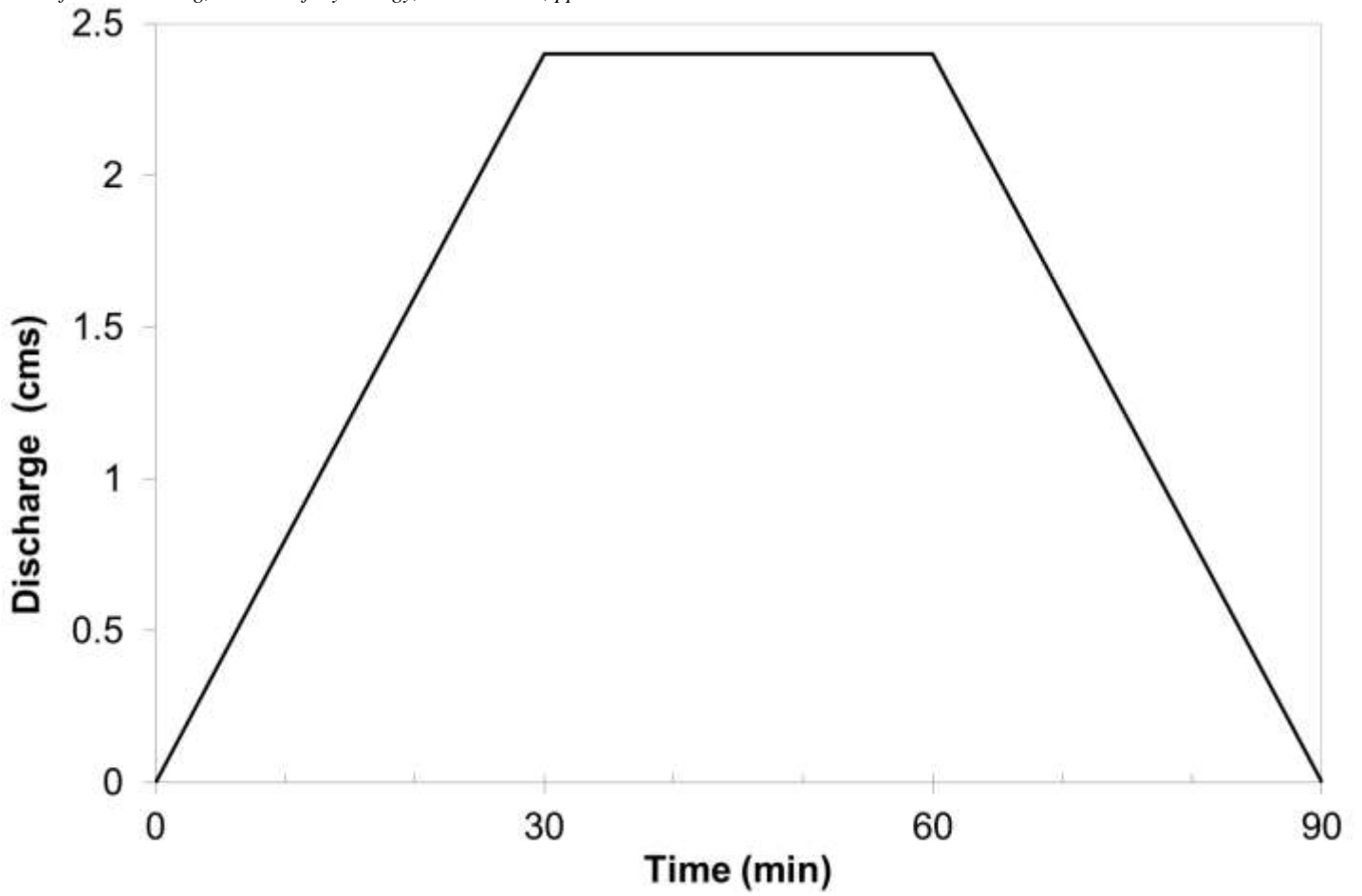
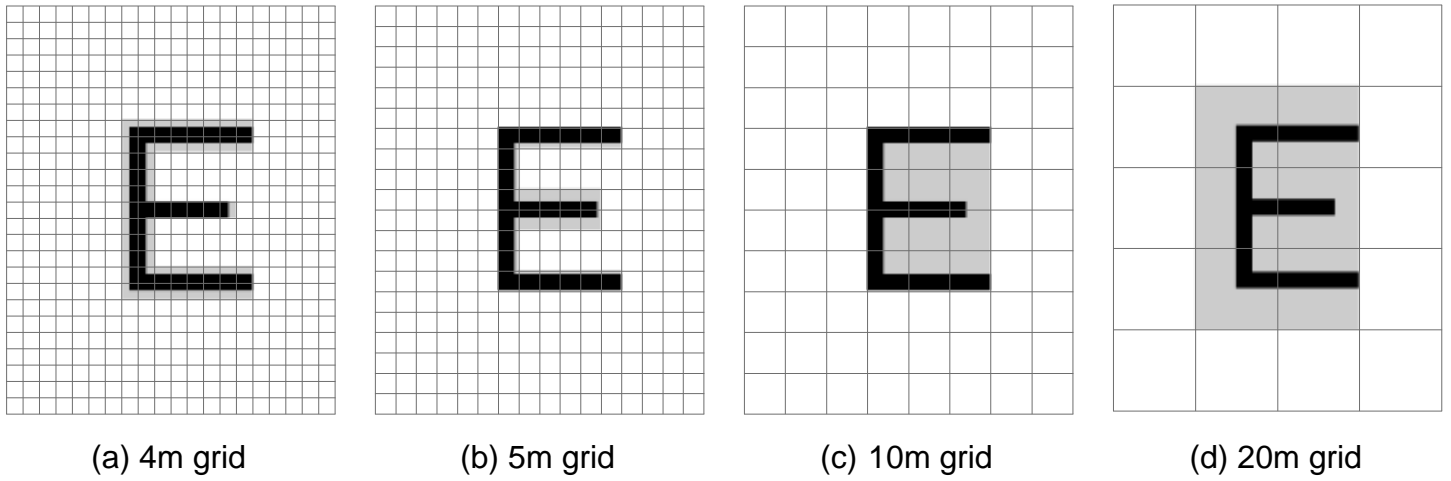


Figure 10. Lateral flow input for E-Building datasets



Legend

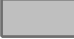


-  Cell boundary
-  Actual building area
-  Additional area for representing building in coarse grid

Figure 11. The grid alignments of the E wall for different resolutions

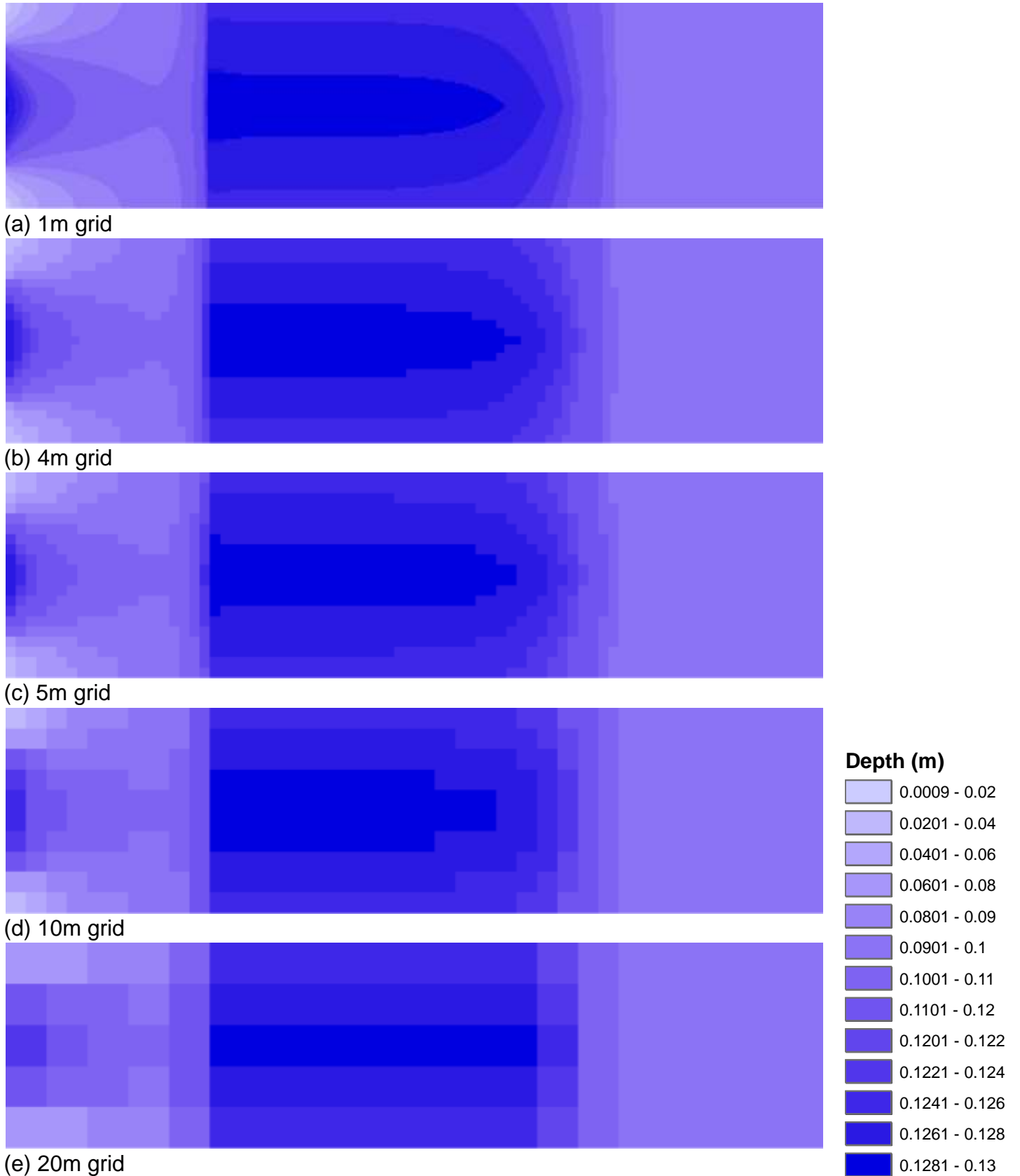


Figure 12. The maximum flood depth distribution of the bare DEM simulations

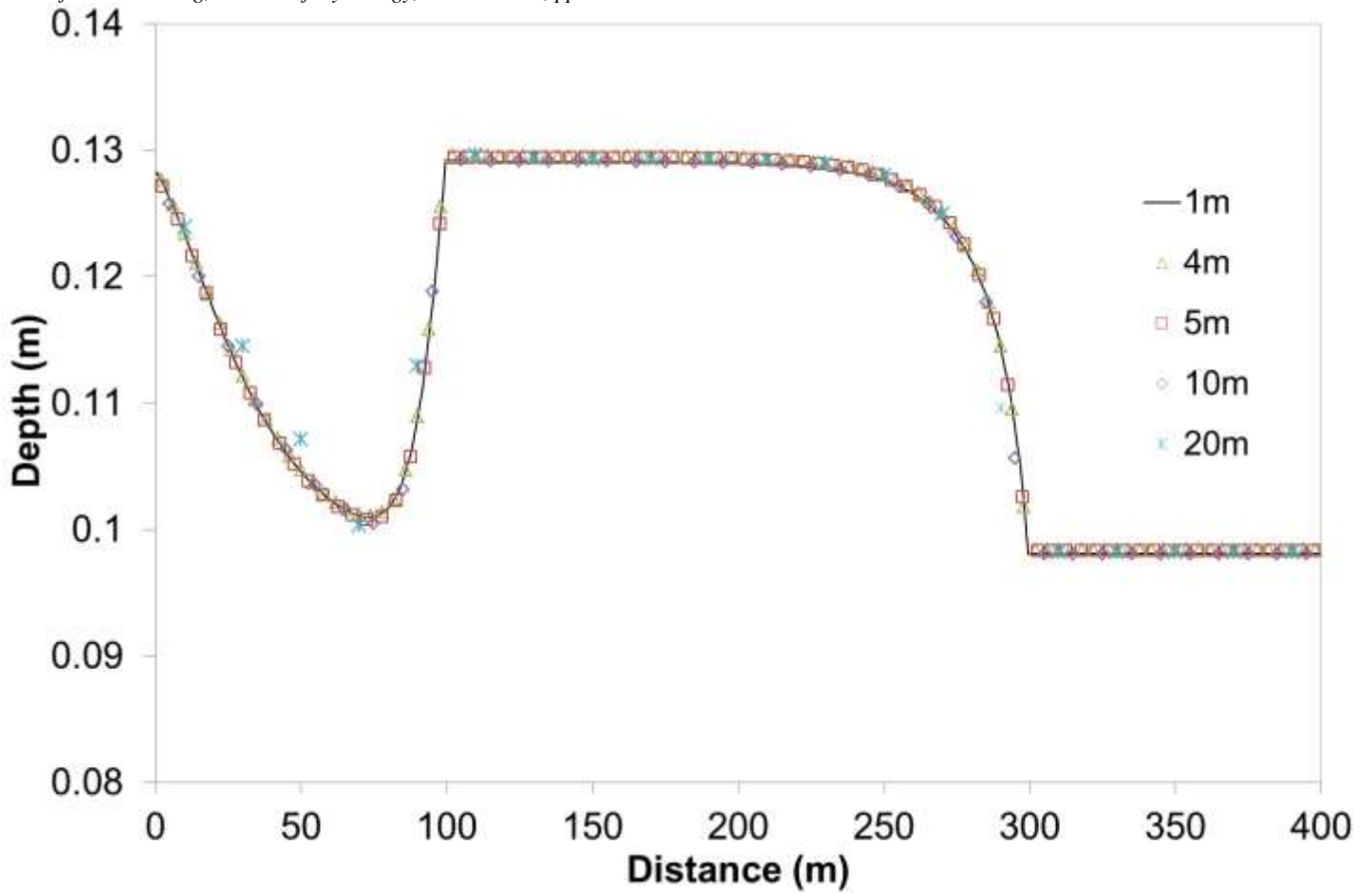
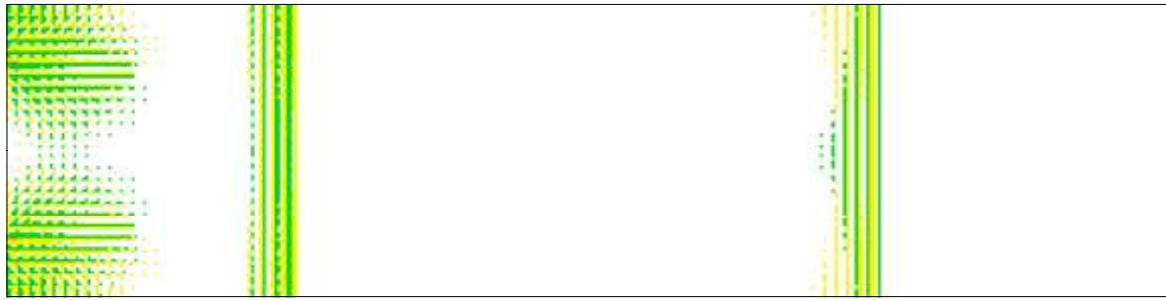


Figure 13. The maximum flood depth profile along the central line in the x direction for simulations of the bare DEM case



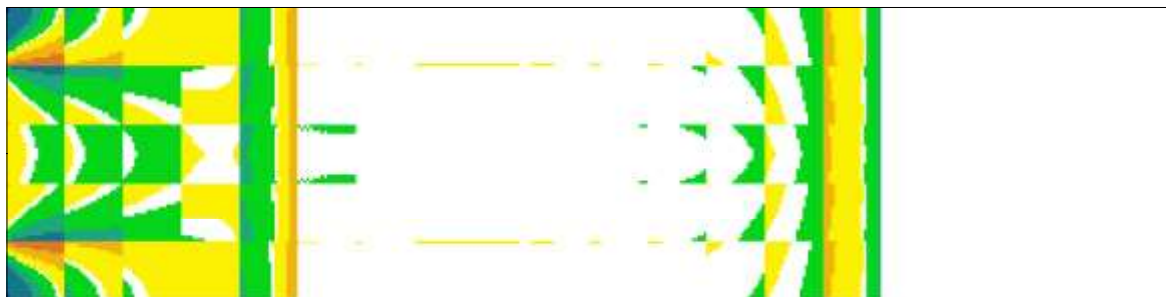
(a) 4m grid



(b) 5m grid



(c) 10m grid



(d) 20m grid

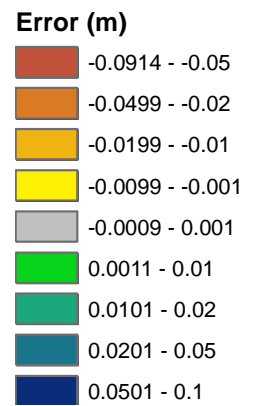


Figure 14. The errors of the maximum flood depths for simulations of the bare DEM case

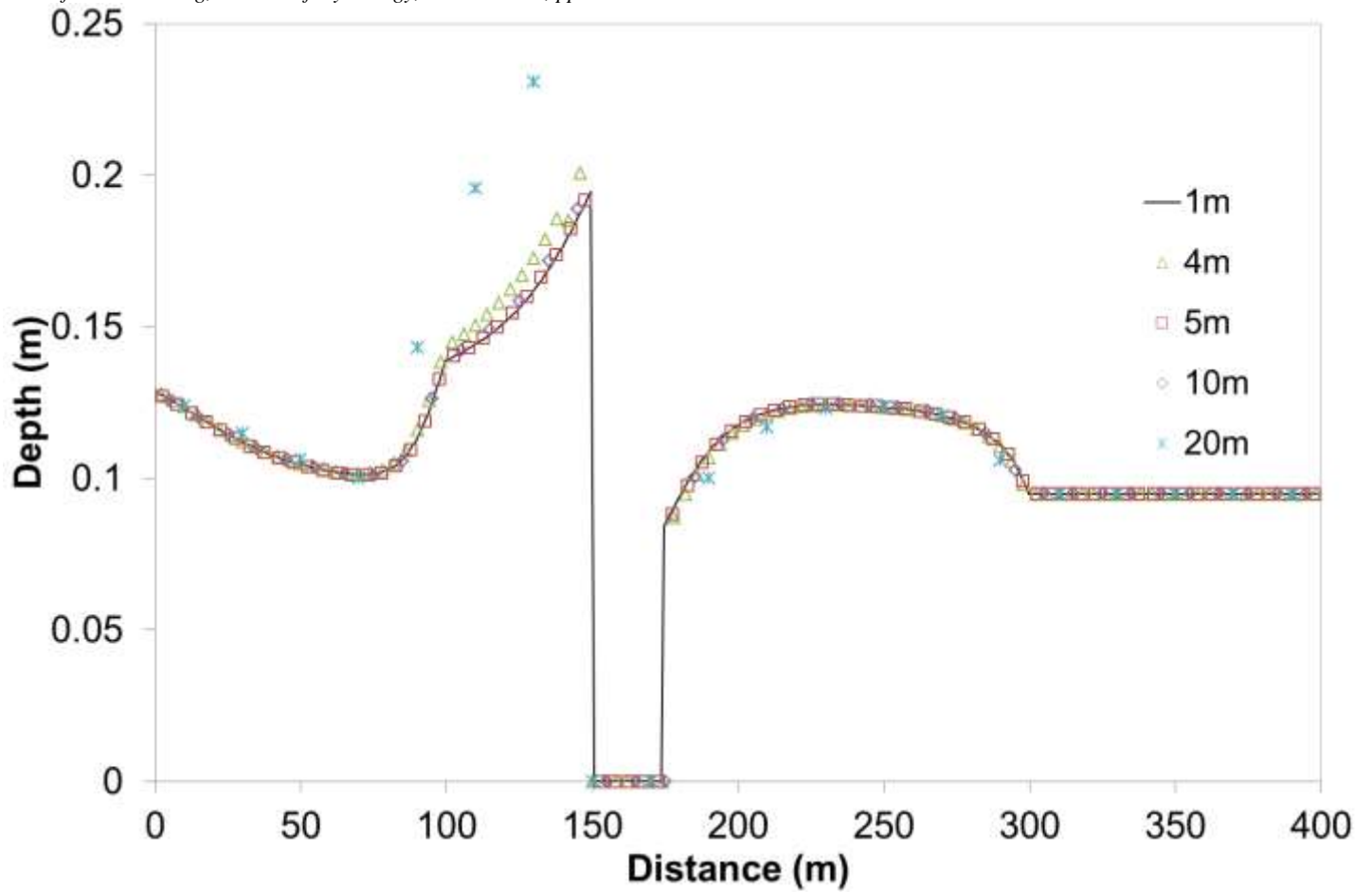
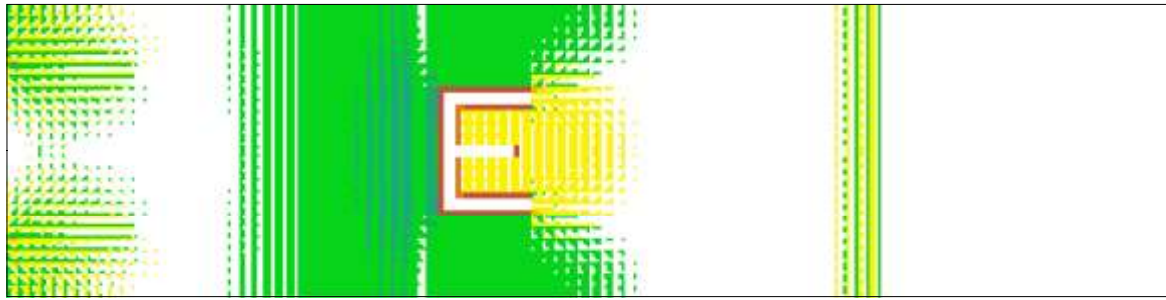
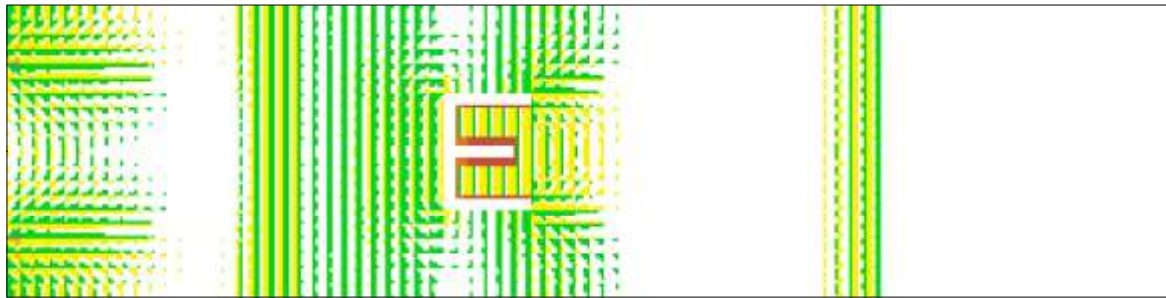


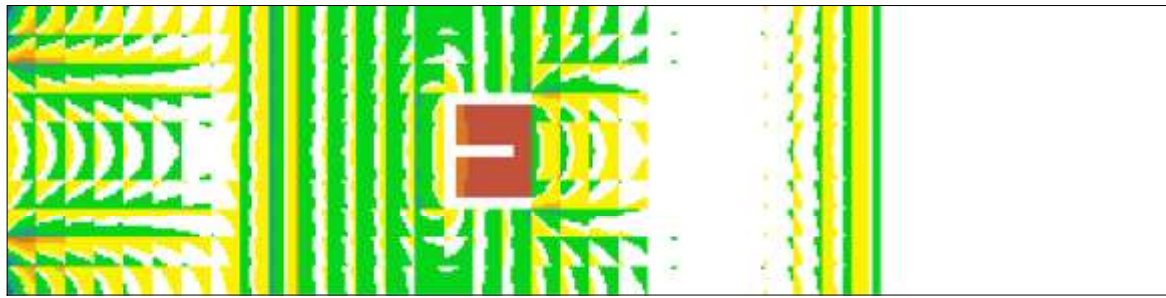
Figure 15. The maximum flood depth profile along the central line in the x direction for simulations of the averaged DEM approach



(a) 4m grid



(b) 5m grid



(c) 10m grid



(d) 20m grid

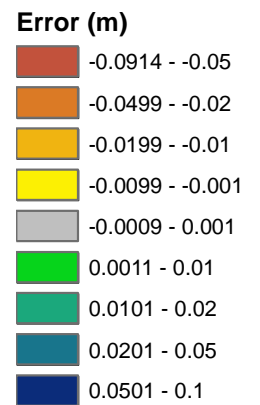


Figure 16. The errors of the maximum flood depths for simulations of the averaged DEM approach

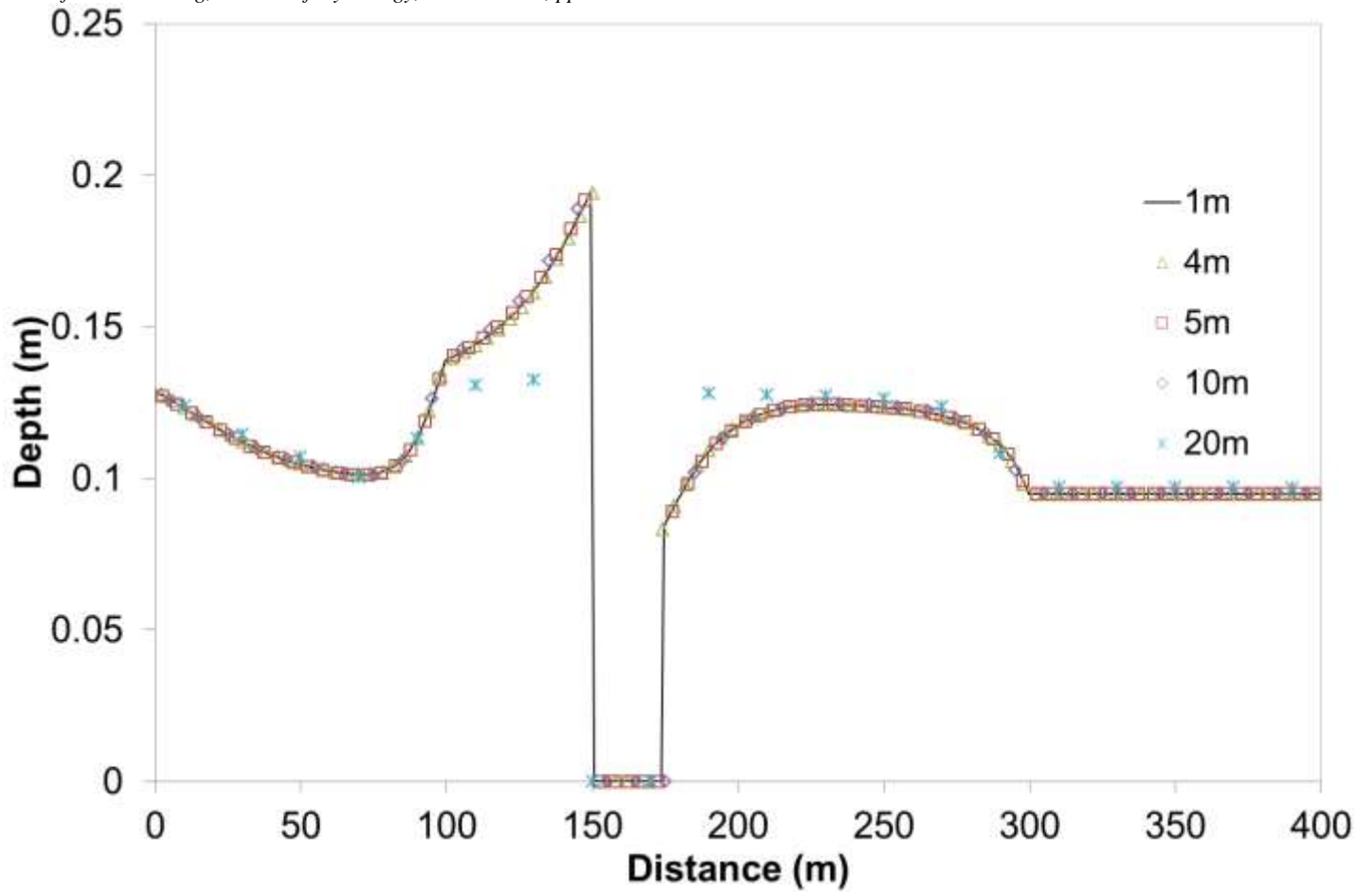
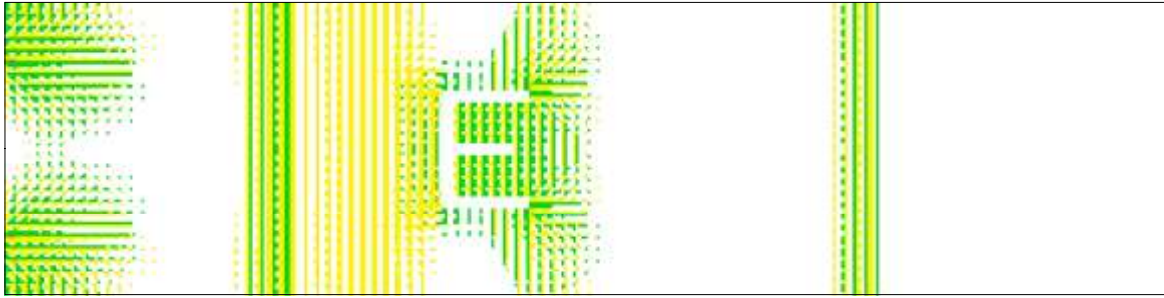
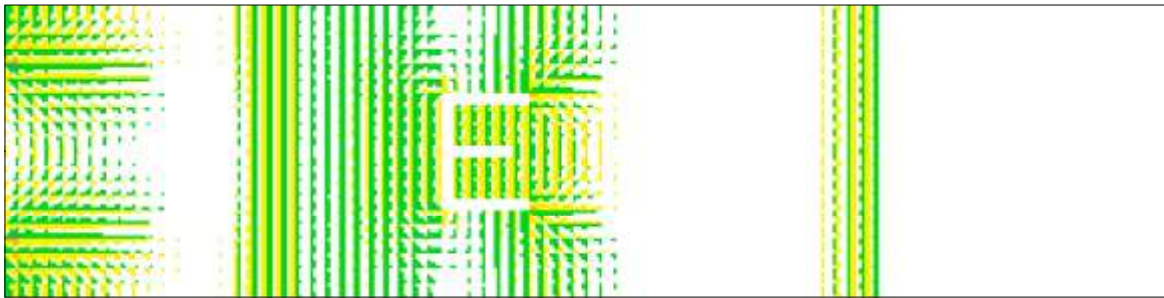


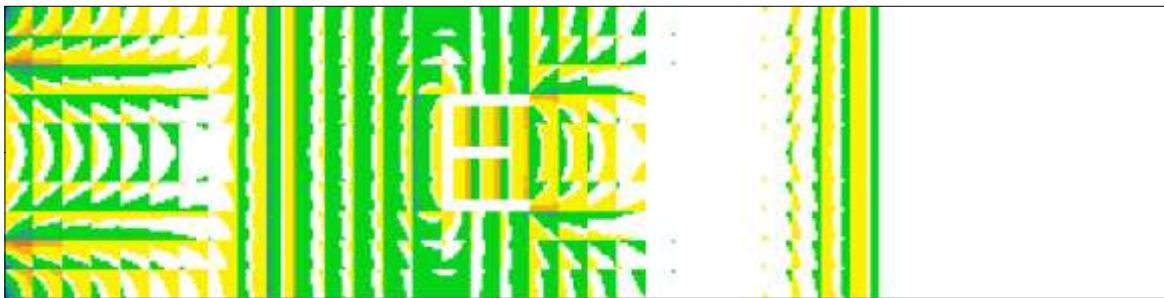
Figure 17. The maximum flood depth profile along the central line in the x direction for simulations of the BCR & CRFs approach



(a) 4m grid



(b) 5m grid



(c) 10m grid



(d) 20m grid

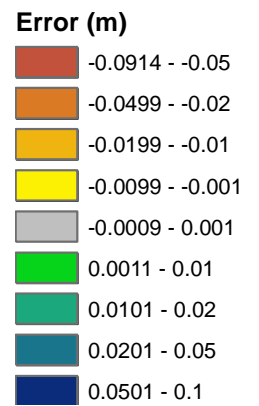


Figure 18. The errors of the maximum flood depths for simulations of the BCR & CRFs approach

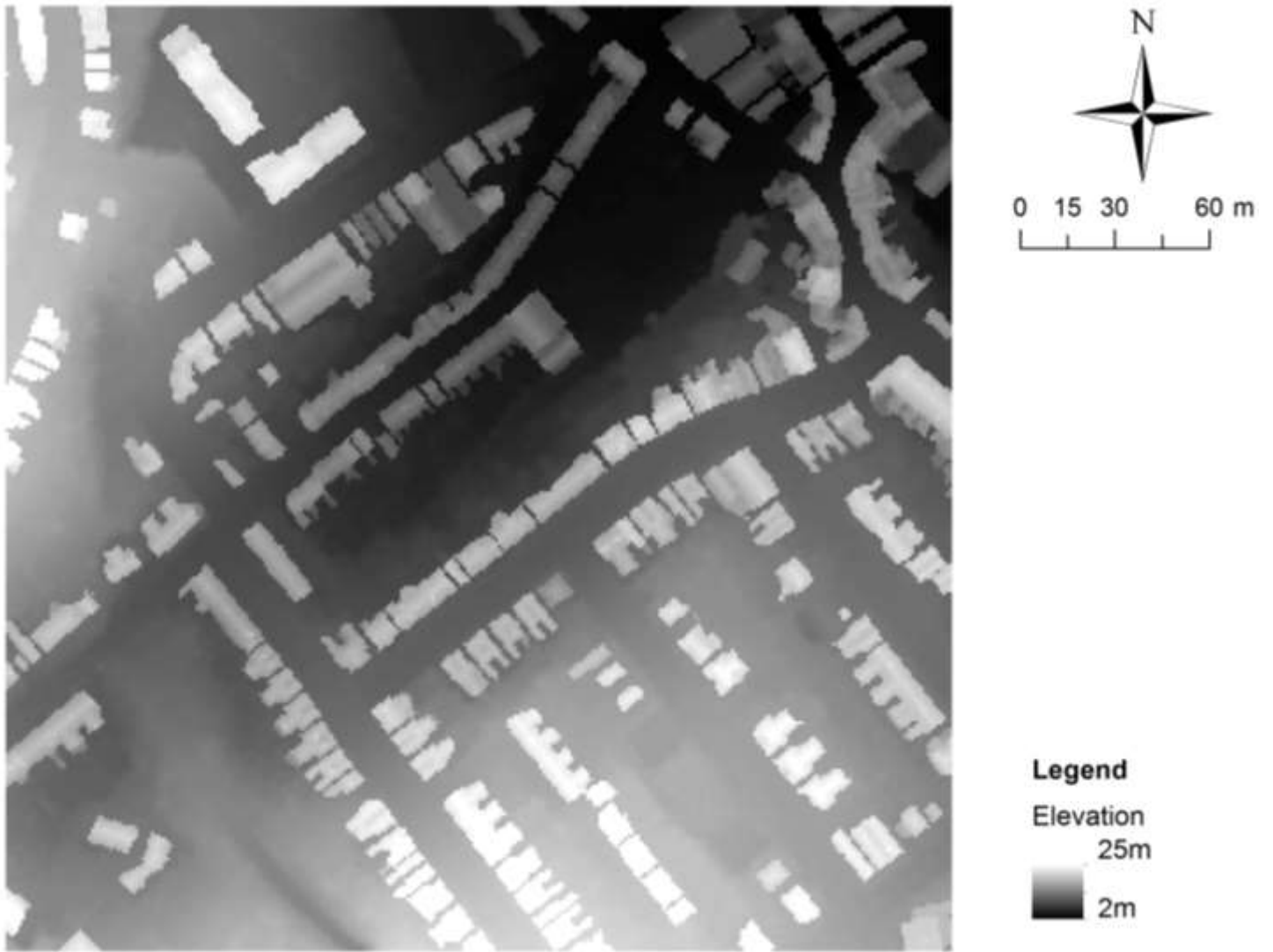


Figure 19. The terrain elevation with building height LiDAR sample

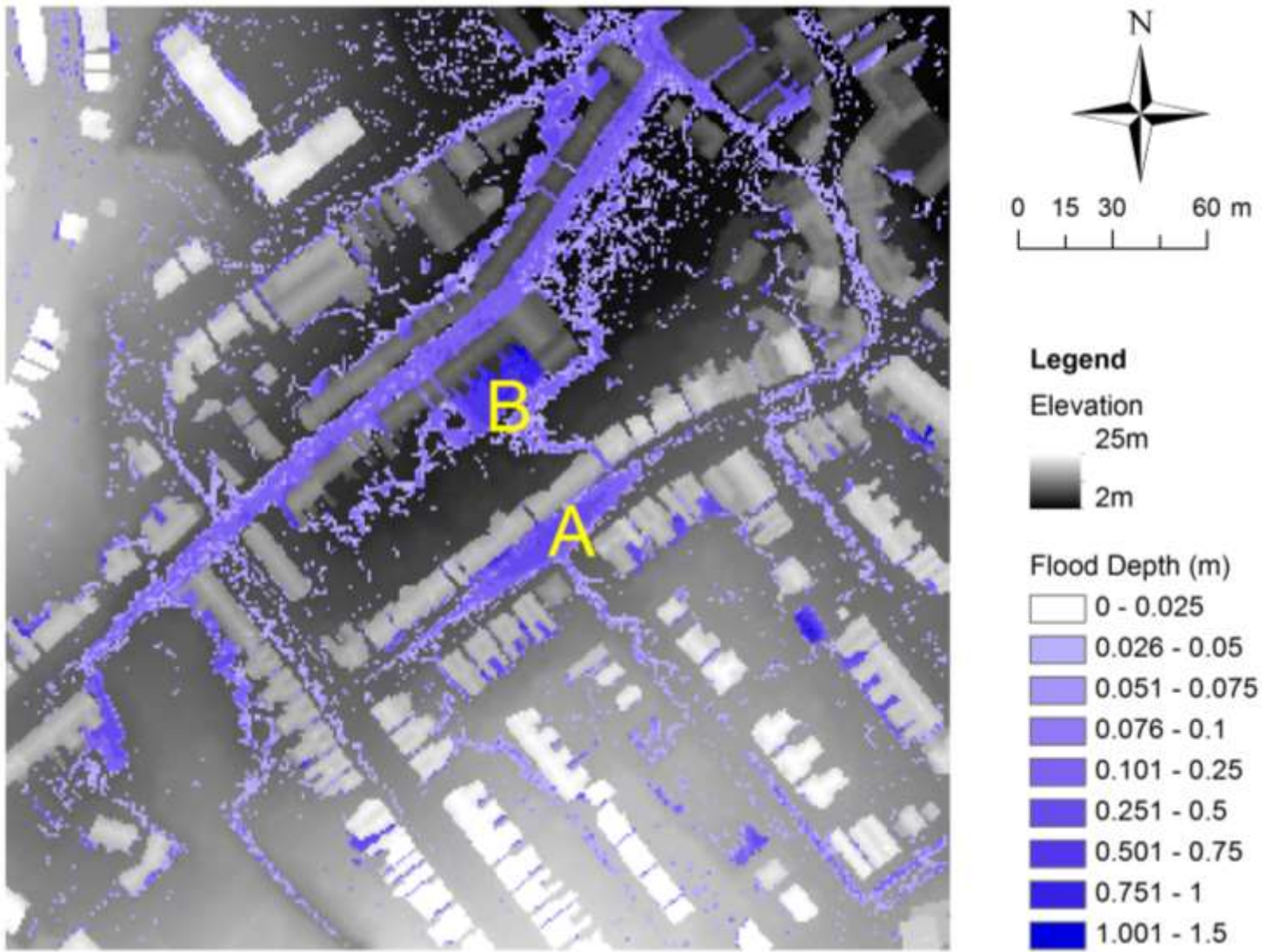
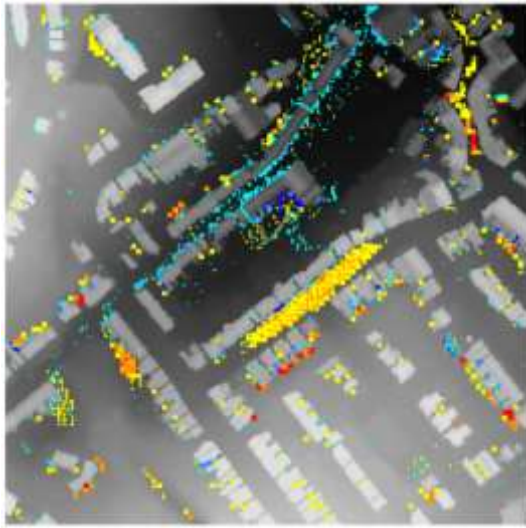
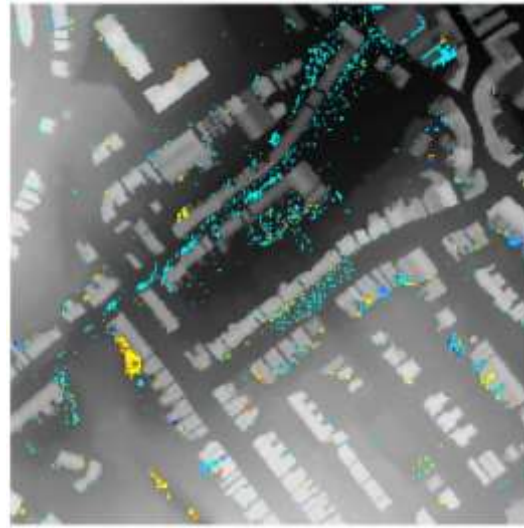


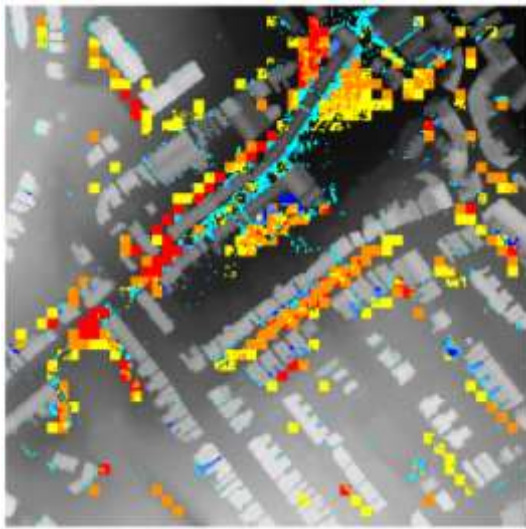
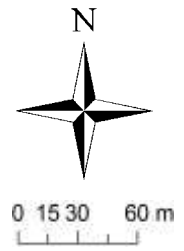
Figure 20. The maximum flood depth obtained from 1m benchmark modelling result



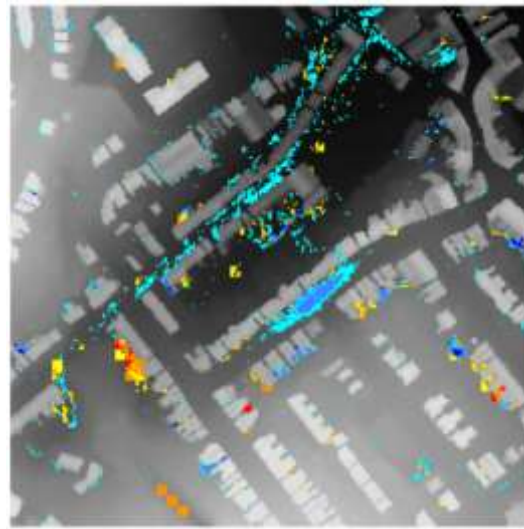
(a) 3m averaged DEM



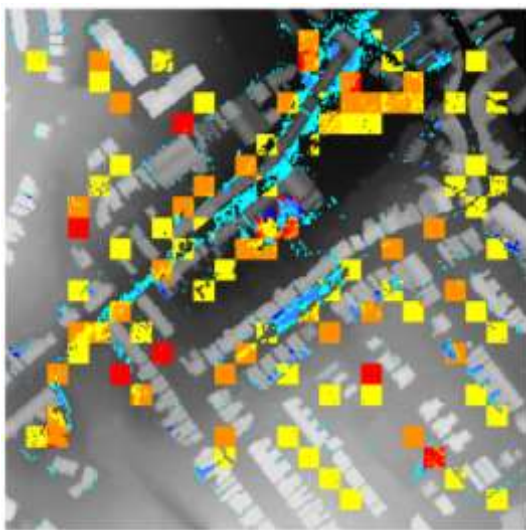
(b) 3m BCR & CRFs



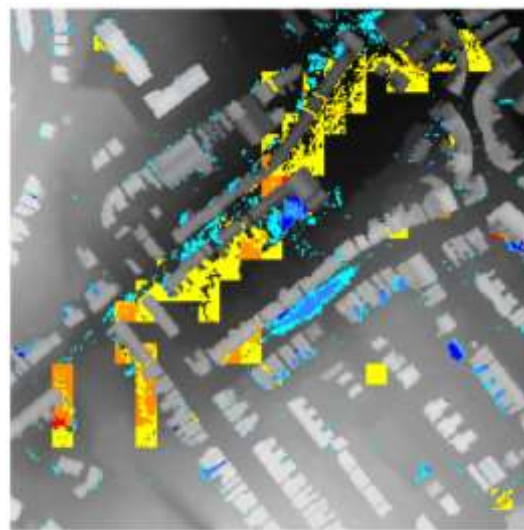
(c) 6m averaged DEM



(d) 6m BCR & CRFs



(e) 12m averaged DEM



(f) 12m BCR & CRFs

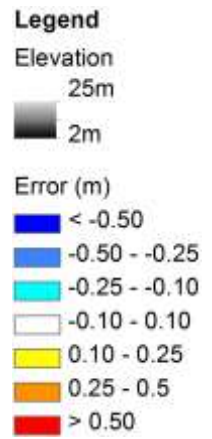


Figure 21. The errors of the maximum flood depths for simulations of the averaged DEM and the BCR & CRFs approaches of coarse grids against the 1m benchmark solution

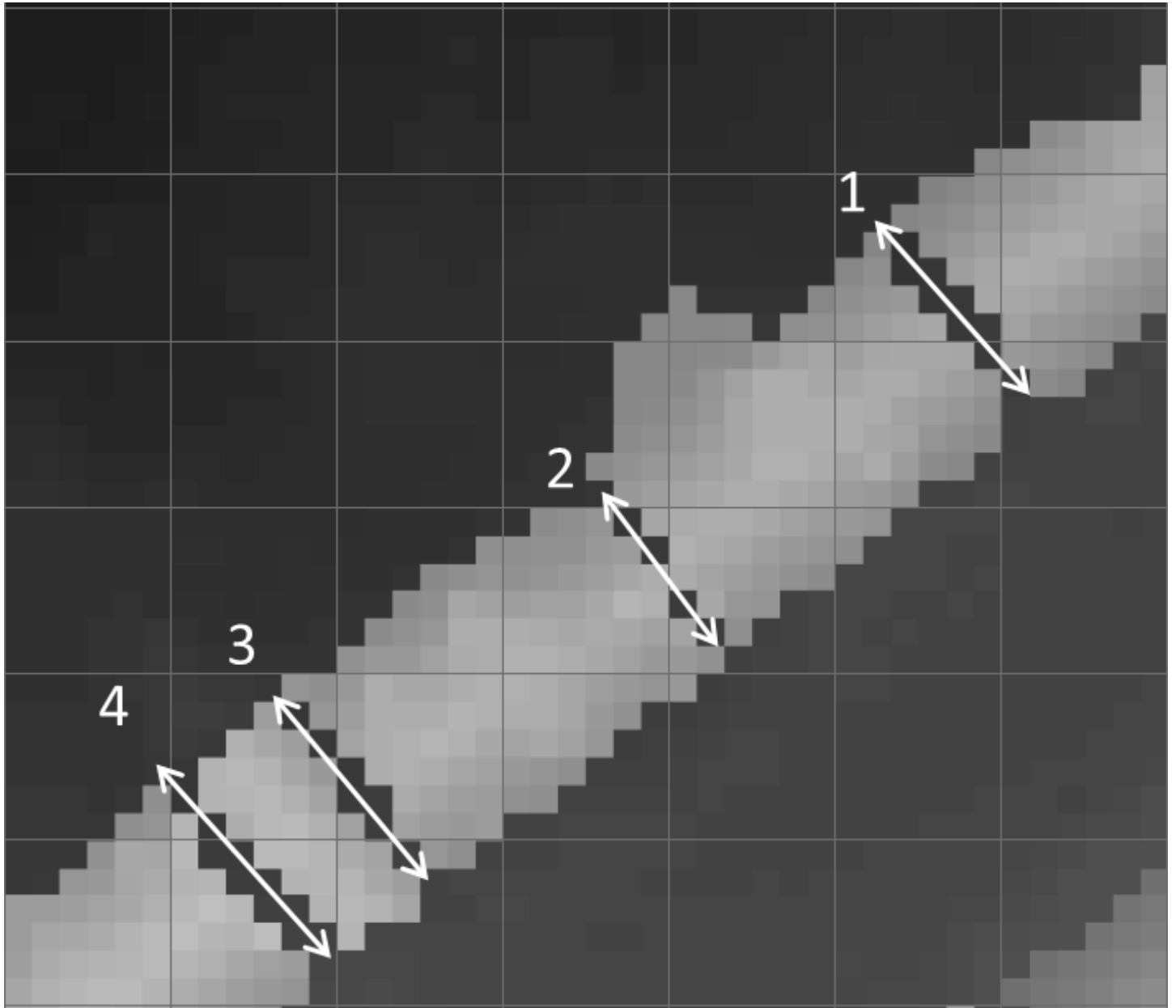


Figure 22. Flow in coarse cells through previously closed alleyways next to region A

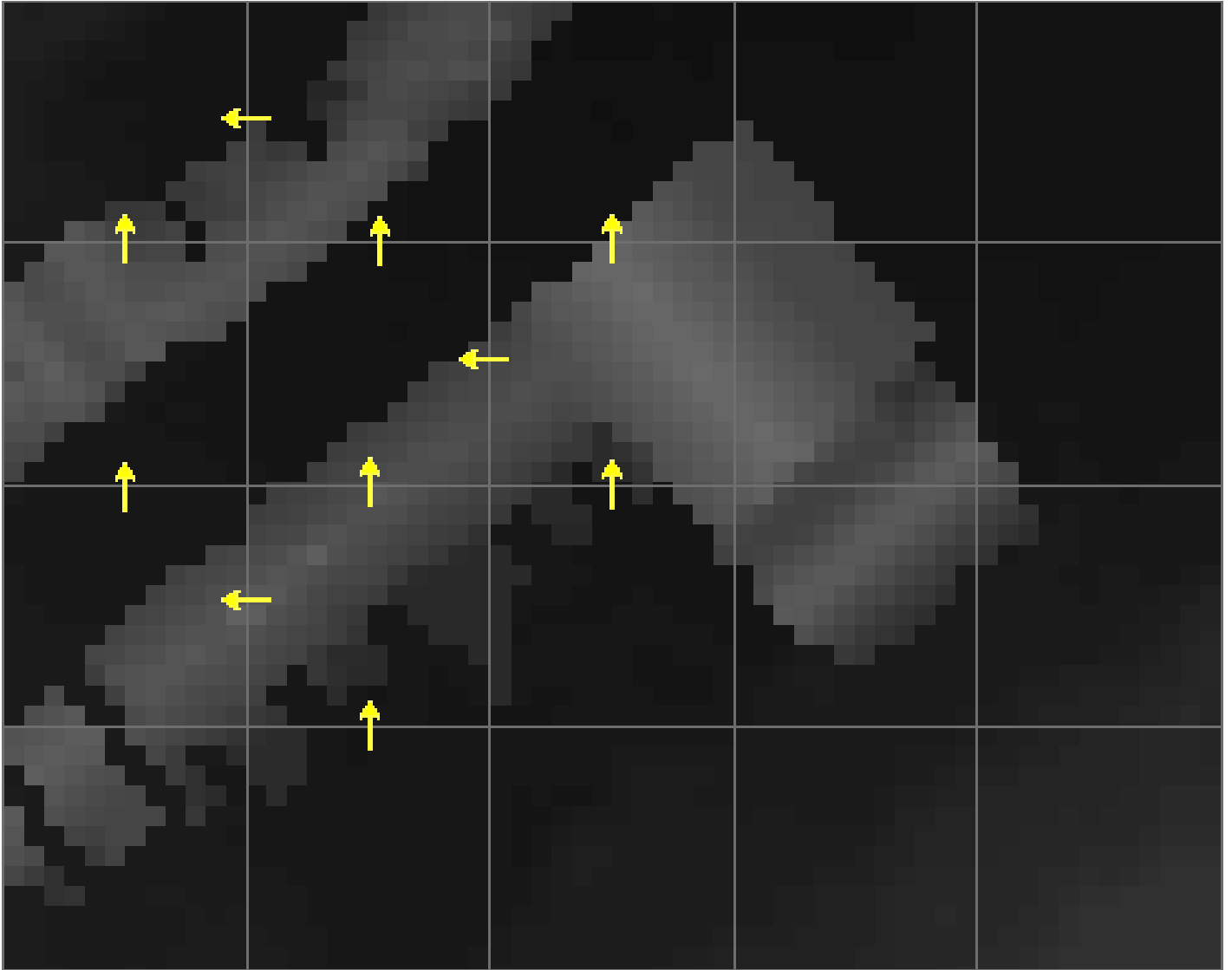


Figure 23. Erroneous flow routing through buildings for region B in the BCR & CRFs approach

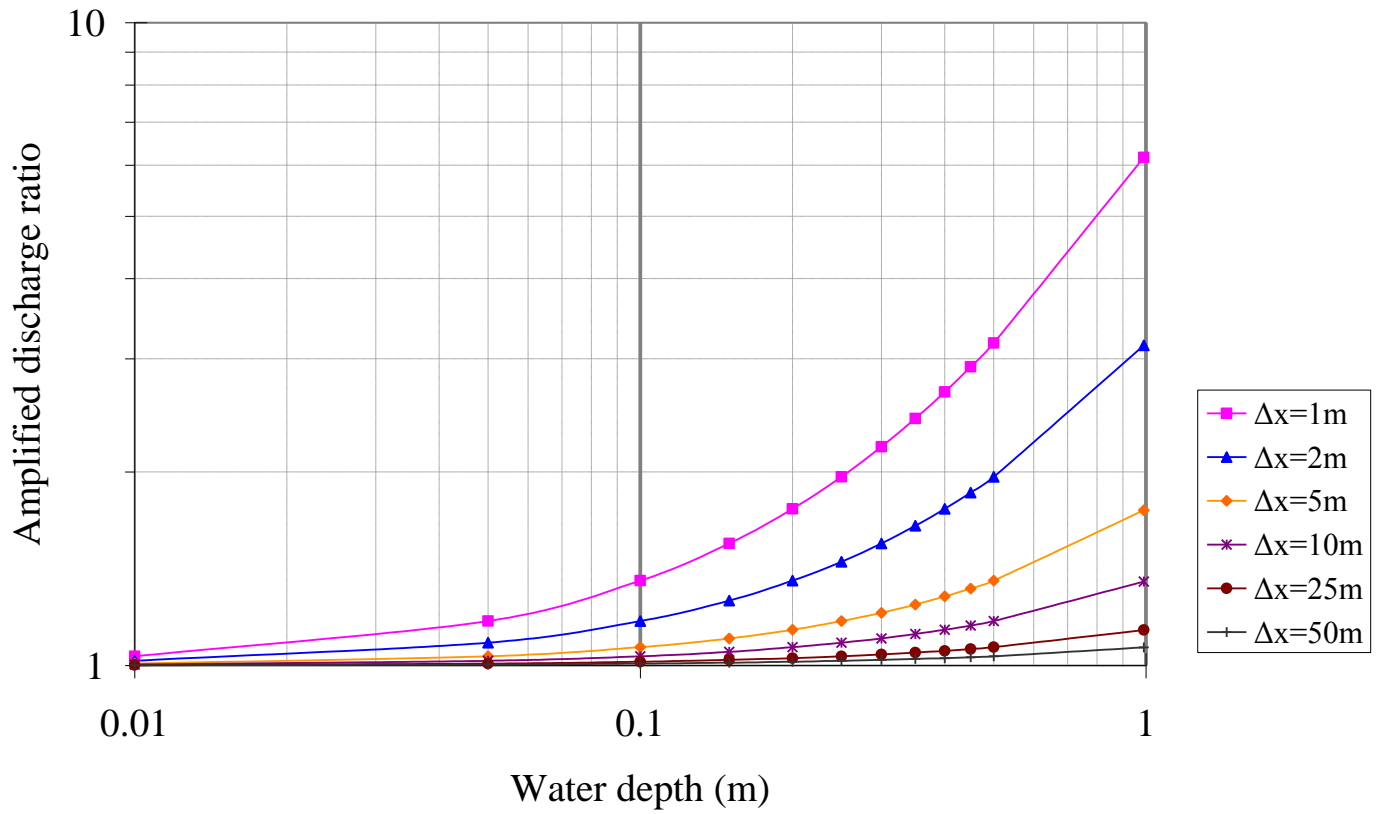
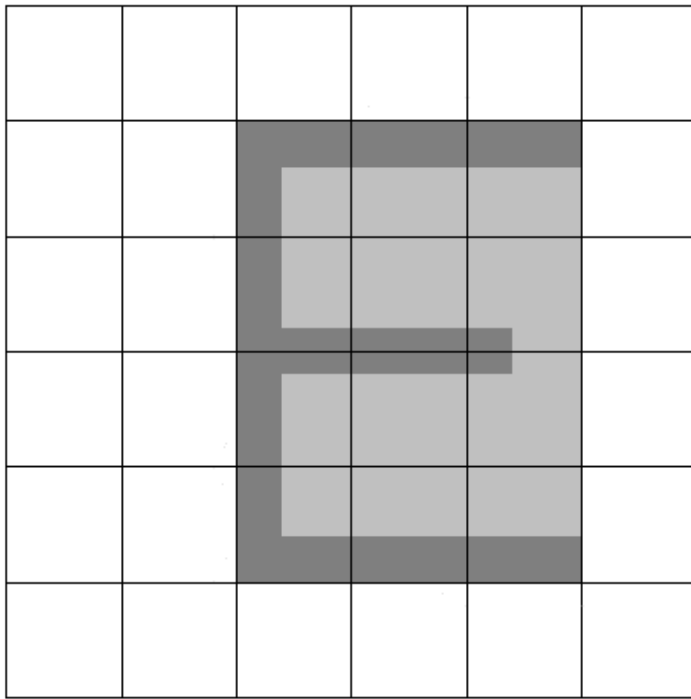
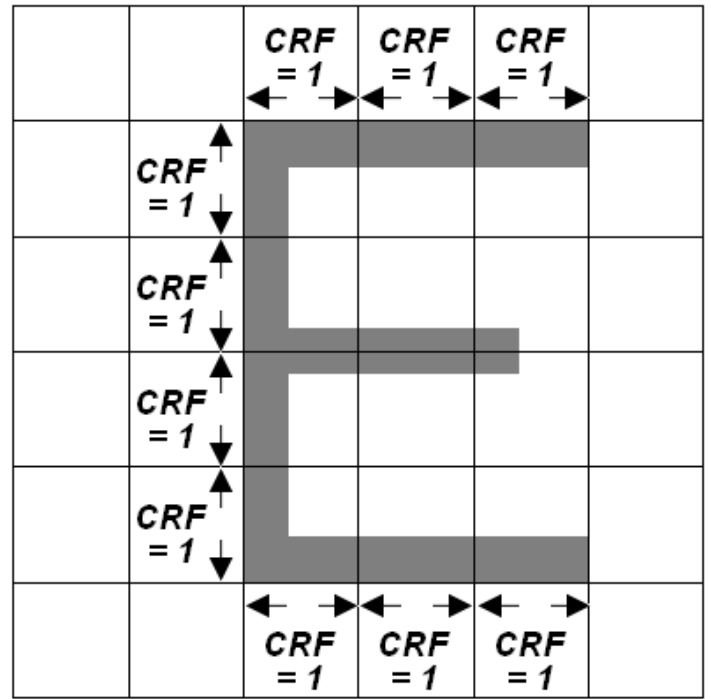


Figure 24. The amplified discharge ratio, for different grid sizes, when the hydraulic radius is replaced by the water depth

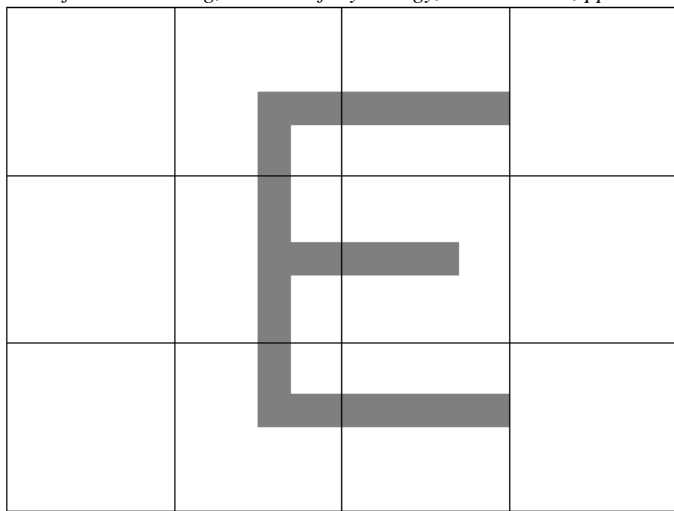


10m Generalised case

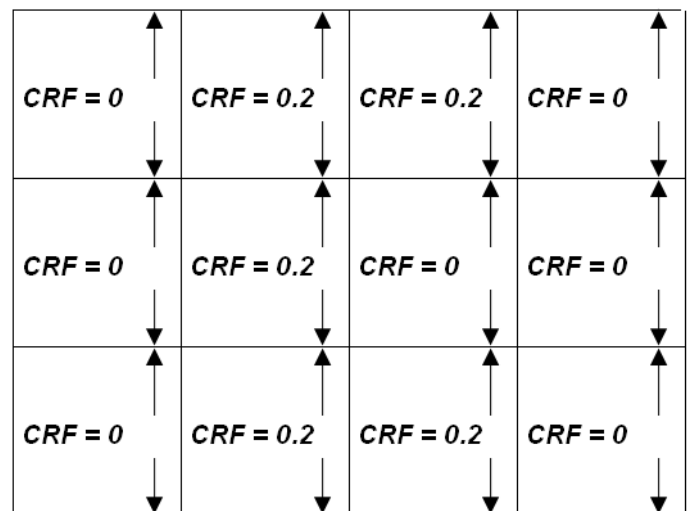


10m Single layer case

Figure 25. The CRFs on the cell interfaces on building edges in 10m grid modelling



20m window overlaid on building layout



CRF_x values for 20m single layer grid

Figure 26. The CRF_x values on the cell interfaces on building edges in 20m grid modelling